# BSc. Thesis

## Electronic markers for geological research

D.A.E. de Gruijl (4568567)
M. Kraaijeveld (4567862)

**Tag Design**

TU Delft

# BSc. Thesis

## Electronic Markers for Geological Research

Bachelor Graduation Project
at the Delft University of Technology.

| | | |
|---|---|---|
| Project duration: | April 1, 2019 – July 6, 2019 | |
| Supervisor: | Dr. ir. G. de Graaf | |
| Proposer: | Dr. M.E. Donselaar | |
| Jury: | Dr. A. Endo | |
| | prof.dr.ir. A.J. van der Veen | |
| Collaborators: | D.A.E. de Gruijl | (4568567) |
| | M. Kraaijeveld | (4567862) |
| | A.S. Roos | (4536827) |
| | M.A. Postma | (4563638) |
| | D. de Groot | (4607414) |
| | E.R. van der Meijs | (4567528) |

TU Delft

# Abstract

In this thesis, the implementation of a passive, chipless, frequency coded Radio-Frequency Identification (RFID) tag for bedload transport studies is proposed. The proposed tag will be deployed in the semi-arid Río Colorado river, Bolivia with the aim to develop quantitative sediment transport models that relate transport to grain size. The designed tag is an open-loop resonator with a fragment-loading structure, that has an optimised configuration based on a Multiobjective Evolutionary Algorithm based on Decomposition combined with Enhanced Genetic Operators (MOEA/D-GO).

The designed RFID tag can ideally reach a size of 4 by 4 millimetres with a maximum calculated reading range of 1.3 meters, and operates in the ultra wide band from 3 to 7 gigahertz. Numerous simulations on the tags were run to verify their properties. The tags proved to have a good directivity, quality factor and radio cross section on its resonant frequency. The tags could reach resonance frequencies as low as 2.9 gigahertz and quality factors as high as 130. The proof of concept on a Printed Circuit Board with an FR-4 substrate results in a tag of 6.4 by 3.4 millimetres. Unfortunately, these properties could not yet be verified by measurement.

# Preface

Sediment transport studies are essential to understand how natural structures are created, modified or destroyed. As a part of these studies, integrated quantitative models of sediment routing systems are made. The tracking and tracing of individual sediment particles is of key importance in the construction of these models. Since its existence, research has been conducted in a variety of ways. In the last two decades, the use of RFID technology has become more viable and preferable for the ability to individually distinguish between tracers. However, the size of current RFID tags limits the research to tracking only larger sized sediment. The aim of the Bachelor Graduation Project (BAP) is to develop a system that would allow the further down scaling of a tag to eventually be able to gather quantifiable measurements on the transport parameters of sand-like sediment. The product is initially developed to aid in the evaluation of the pristine Rio Colorado sediment-routing system in the semi-arid, sparsely-vegetated Altiplano Basin of Bolivia in a joint research between KU Leuven and Delft University of Technology.

Firstly, we would like to thank Dr. M.E. (Rick) Donselaar for proposing this project. Dr. Donselaar has given us great insights into the importance and applications of sediment tracing studies, which has proved to be of great importance for this project. Secondly, we would like to thank dr.ir. G. de Graaf for his supervision during this thesis. His guidance has helped us immensely in structuring the project. We would also like to thank ir. P.J. (Pascal) Aubry for helping us set up UWB measurement setup. Morevover, Prof. Alexander Yarovoy is appreciated for his effort in structuring the problem and assisting us with possible solutions.

The tag design group would like to thank the PVMD group, and in particular dr. Olindo Isabella and ir. Rezaei for granting us access to their server room. Finally, we should also thank mr. Frehe for helping us out with IT related issues.

# Contents

# 1 Introduction

Since the beginning of time, rivers have shaped landscapes in extraordinary ways. To understand how rivers form and function, bedload transport studies are of key importance. Data collected from these studies can be used to further develop general sediment transport models. The goal of these models is to eventually be able make statements about the sediment transport of an arbitrary river. Changes in sediment quantity and quality can not only have effect on the environment, but also on social and economic systems [1]. Examples of this include research on the behaviour of the Kulim River in Malaysia, which floods frequently [2].

To construct quantitative integrated models for sediment routing systems, the ability to track and trace individual sediment particles in space and time is essential. Serious tracking studies started with the tracking of radioactively tagged particles in the 1950s. This method cannot be used in most situations because of health and safety issues. Other methods include the use of fluorescent glass and magnetic material. The fluorescent glass is able to be detected at range using UV light and the particles are able to be sized down to 44 $\mu$m. It has however only been used in simulations on laboratory scale [3]. The magnetic material is arguably more cumbersome requiring soil samples both before and afterwards, as well as knowledge of loss of magnetic characteristics of the material used [4]. Neither of the methods mentioned above have the option to deploy individually distinguishable tags.

In the last two decades, a growing number of researchers made use of radio frequency identification technology to research bedload transport [5]. This method is advantageous as it allows tracers that are relatively cheap, durable and can be distinguished by unique codes [6]. The unique code of RFID tags allows to track individual displacement of particles, which allows for more complex modelling of river systems.

RFID systems consist of a reader or scanner and a transponder or tag. When exited, the tag transfers data to the reader. This can be done in two ways: transferring through a magnetically coupled circuit located in the near field, or using a send and listen method with the tag and reader placed in each others far field region [7]. The currently used systems are low-frequency tags working in the near field, achieving ranges up to about 40 centimetres [6]. The tags used are passive and contain a chip which is harvesting the energy from the electromagnetic waves from the reader. When sufficient energy is harvested, it is used to power the on board integrated circuit which in turn will send out an electromagnetic (EM) signal which, when received, can be used to identify the tag. The typical size of these tags is about $20-30$ millimetres [6]. Similar RFID technologies are used for different research subjects. For example, to study the behaviour of bees. In this case, RFID tags have been placed on the bees with the readers placed at the entrances of the hive [8]. Again the chips where passive and with a chip, sized $3.1 \times 1.6 \times 0.5$ millimetres, achieving a reading range of about 5 millimetres.

This thesis focuses on the development of an RFID system used for sediment research in the Río Colorado, Bolivia [9]. The Río Colorado is special in the regard that it is a very simple river to model. It has one source and one sink, and mouths into a shallow salt lake. The river is semi-arid, as many rivers are on this globe and the region has little to no vegetation, which simplifies the modelling of rain water. Sediment research calls for uniquely identifiable tags that reach the size of sand grains. Current technology is either uniquely identifiable

or as small as sand, but not both. On the same token, technology should remain cheap and durable. The gap in this technology poses limits to sediment transport models that can be constructed, as is the case in rivers around the world.

This poses the following design challenge:

> Design uniquely identifiable tracers that behave like sand grains through a riverbed.

It is argued that the solution is a chipless, passive RFID system using Vivaldi antennas for detection and digital signal processing technology in the frequency domain in combination with a global positioning system (GPS). This particular thesis has its focus on the design of the RFID tag. For the design of the other system components, one should consult the work of Roos, S. and Postma M.A. [10] and Van der Meijs, E. and de Groot, D. [11].

In chapter 2, the exact requirements of the system will be laid out. In chapter 3, the design of the entire tracking system will be described. In this chapter, some of the basic design choices are explained. The design of the RFID tag will be explained in chapter 4. Simulations and verification of the design can be found in chapter 5. Subsequently, in chapter 6 the realisation and testing of the RFID design is reported. Finally, the discussion and conclusion is written down in chapter 7 and chapter 8.

(a) Grass-covered bank in the upstream area

(b) Non-vegetation bank in the downstream area

Figure 1.1: Upper coastal plain [9]

# 2

# System requirement analysis

With the design question:

> Design uniquely identifiable tracers that behave like sand grains through a riverbed.

only a broad goal for this project is established. No concrete requirements are apparent. With the aim to solidify and specify the objective a couple of meetings with Rick Donselaar were scheduled to discuss his needs regarding sediment tracing and the nature of the underlying problem. From this point a success scenario was written, from which direct functional and non-functional requirements can be derived following the template by Bahill and Dean [12].

**Use case name:** Geological research using Electronic Markers

**Main success scenario**

1. Distinct tags are distributed over the river bedding at known locations.
2. The rain season starts and the tags drift downstream behaving exactly like the sediment they were placed in.
3. The rain season passes and the river dries up.
4. The measurement device is attached to the vehicle.
5. The vehicle moves at low speed through the river bedding.
6. Tags are located and their respective locations are placed in a spreadsheet
7. The locations are analysed by the researcher.
8. Every tag may stay in the river and is able to be detected again for further analysis after next rain season.

**Functional requirements**

**F1.** The tracers should be detected wirelessly.

**F2.** The tracers should be uniquely identifiable up to a 100 devices.

**F3.** The tracers should behave as sand grains on a riverbed.

**F4.** The tracers should be able to withstand salty water.

**F5.** The tracers should be detectable from a vehicle.

**F6.** The tracers should be detectable from a minimum of 40 cm while buried up till 5 cm in sand.

**F7.** The measurement setup should be transportable through the riverbed.

**F8.** The measurement system has to function in a temperature range between -10 and 40 degrees Celsius.

**F9.** The tracers should withstand temperatures in a range -20 and 50 degrees Celsius.

**Non-functional requirements**

**N1.** The system should present collected locations in a straightforward way.

**N2.** The tags should be recoverable or non-harmful to the environment.

**N3.** The system should be save for people to work around.

**N4.** The system should comply with relevant organisational and governmental regulations.

# 3

# System Design

On the basis of this project, three theses will be written. To understand how each thesis will be structured, preliminary design choices have to be made. In this chapter, these design choices are substantiated. First, a short recap will be made on why an RFID system was chosen. Then, the choices and considerations in RFID systems will be explained. Subsequently, a number of possible designs will be laid out, based on their working principle, an exemplar implementation, the expected performance and its feasibility within the context of the project. Finally, a design choice will be made and its general system will be further explained. This system is split into three subsystems, which will each be one thesis.

## 3.1. Types of technology

A number of different sediment tracing methods are currently used to track sand-like material. They are generally divided into two groups [3].

1. Labelled (coated) natural particles
2. Labelled synthetic particles

Associated with the first group are for instance natural particles labelled with fallout radionuclides, fluorescent paints and fingerprinting techniques [4]. Due to their primitive nature they lack the ability to be individually distinguishable. With advancements in technology the production of synthetic particles became feasible. This allowed for the use of materials that facilitate the detection of the tracers more consistently. The common tracers used in this category are rare earth elements (REE) tracers, magnetic substances and polystyrene plastics [3]. These types of traces do have the ability to be distinguishable between sets using chemical processes that are rather cumbersome and require soil samples [4]. More recently, RFID has also been used to track larger sediment particles, e.g. boulders, cobbles and pebbles [6].

## 3.2. Choice for RFID

There is a significant difference between the use case of previously used RFID tracers and the one of the design problem described in this thesis. The locations of the tags in Bolivia are only measured outside of the rainy season, when the riverbed has run dry. As a result the use of EM waves becomes an option because attenuation through water no longer poses an issue. RFID technology that allows for individual identification has already been used to research group behaviour of bees. However, the devices used in this research have a relatively small detection range of about 5 mm [8].

Compared to the previously used technologies RFID seems to be more in line with the requirements. Therefore, the first major decision is to pursue detection of the particle based on RFID technology.

## 3.3. RFID technology

Since the choice has fallen on RFID in section 3.2, a choice needs to made which type of RFID coding will be used. This coding type will determine all specifications and parameters for all subgroups, and is therefore of key importance. This section will describe the various RFID technologies which were under consideration.

### 3.3.1. Active and passive designs

In RFID tracking systems, there are two major technologies that can be defined: passive and active tracking. Passive RFID tags have no internal power source. Active RFID tags are battery-powered and are able to broadcast their own signal continuously. They are more often used for continuous tracking, have a long read range and are more expensive. Passive tags are cheap and small, but their range is limited, since no extra energy from an internal source can be drawn to send back a stronger signal to the reader [13].

To design the RFID system, a few requirements were taken into account. First of all, the tag should be as small as possible, preferably as small as grains of sand. This puts enormous stress on the design of a battery system if an active RFID system should be realised. Secondly, the price is taken into account. The tags should be as cheap as possible, because they are deployed in large numbers. Passive tags are cheaper than active tags, since their design is often simpler. Thirdly, passive tags can last a lifetime without a battery, depending on the wear and tear. This is not the case for active tags. Since the sediment research is done over several years, it is important that the tags can operate for several seasonal cycles.

### 3.3.2. Chipped or chipless design

A passive tag can be implemented in two ways: with or without an embedded chip. The chipless tags are made by creating conductive structures on a substrate in such a way that it will generate a time- or frequency domain signature when it is exited with RF energy [14]. Integrated circuit (IC) based systems mostly use backscattering by changing the impedance of their antennas. The advantages of chipless systems is that production is much more simple than IC production and thus less costly. But after production the encoded information can not be changed anymore. Systems based on resonant structures also do not need a separate antenna which can provide robustness and size advantages. Chip based systems have the advantage that they can provide more complex functions than just identification, by for example implementing a time delay between receiving the interrogation signal and their response or encryption of the contained data.

### 3.3.3. Time and Frequency Coding

Chipless tags are often categorised into two types [15]. The tags in the first category are either retransmission or time-domain reflectometry (TDR) chipless RFID tags. This category of tags uses encoding in the time domain. Data is not encoded in the antennas itself. Instead, the signal is first received by an antenna, then the signal is transformed or simply delayed, thereafter retransmitted. The important data is often encoded by positioning parasitic elements along a transmission line to create reflections at precise moments.

The tags in the second category are either scattering or millimeter-wave (mmW) image-based chipless RFID tags. In these tags, the antenna itself is a resonating element which causes peaks or dips in the frequency spectrum of the received signal. This type of encoding mainly uses the UWB band (3.1-10.6 GHz), which has significant restrictions on the transmitting power.

The tag is required to have a high quality factor, which means its peak(s) have a very narrow bandwidth, such that it resonates at very specific frequencies. The quality factor also influences how long the tag keeps resonating. A high quality factor gives the opportunity to measure the signal after the initial reflection has been received.

Temporal coded tags often have longer reading ranges than spectrum coded tags. The spectrum coded tags use high frequencies, which limits their range. However, spectrum coded tags have higher information densities, which allow them to reach smaller sizes for the same information stored [15].

## 3.4. RFID link

Every RFID system contains by definition an EM link between the tag and the transponder. Information is sent over this link, but not all signal power will reach the receiver. Moreover, noise will be added to the system and reflected signals can interfere with the signal or even saturate the receiver. A better understanding of these phenomena will be given in this section.

There is a difference between the so-called near-field and far-field RFID technologies. In low-frequency near-field technologies, waves do not actually propagate but only exist as a reactive field near the transmitter. By

modulating this reactive field with the tag, the transmitter can directly 'feel' the modulation and can communicate with the tag. However, the tags to be used for this project must be very small, requiring high-frequency EM waves. For this reason, a far-field RFID system needs to be implemented and the calculations in this section assume far-field propagation.

### 3.4.1. Signal power

In a far-field RFID system, the transponder will send a signal to a tag, which will respond. Because the antennas are not made to be perfectly directional as the exact location of the markers is not known, this signal power will spread out which wastes part of the energy. These power transfer characteristics will be described in this subsection. The RFID system can be modelled as a radar system or a free space transmission link. When an electronic marker system is based on a reflection caused by the marker, the system can be modelled as a radar system. When a system is based on a re-transmission of a (manipulated) transmitted signal, the system can be modelled as a free space transmission link.

**Radar system**

To calculate the received power reflected by an object, the transmitted power density must be calculated first. The power of an isotropic antenna spreads out over a sphere. However, the antenna is not isotropic and transmits more power in a certain direction. This is called the gain $G$. Including this gain, the power density at a distance $R$ transmitted by an antenna can be calculated with Equation 3.1.

$$S_{transmitted} = G \cdot \frac{P_{transmitted}}{4\pi \cdot R^2} \tag{3.1}$$

With the power density, the reflected power can be calculated using the reflective area of the object. The reflective area depends on the physical area of the object. However, the reflective area of the object is also material and frequency dependent. The reflective area in radar theory is described by the radar cross-Section (RCS). Using the RCS $\sigma$, the reflected power can be calculated using Equation 3.2.

$$P_{reflected} = \sigma \cdot G \cdot \frac{P_{transmitted}}{4\pi \cdot R^2} \tag{3.2}$$

The reflected power is again spread out over a sphere and the power density will result in Equation 3.3.

$$S_{reflected} = \frac{P_{reflected}}{4\pi \cdot R^2} \tag{3.3}$$

The received power is this time calculated by multiplying the power density with the effective area of the antenna. However, the effective area of the antenna is not equal to the physical area. The effective area of the antenna in radar theory is described by the effective aperture $A_e$. The received power is calculated using Equation 3.4

$$P_{received} = S_{reflected} \cdot A_e \tag{3.4}$$

The effective aperture is not easy to determine for all antennas. However, the gain is known by simulation or measurement. The relation between the effective aperture and the gain of an antenna is given by Equation 3.5.

$$A_e = G \cdot \frac{\lambda^2}{4\pi} \tag{3.5}$$

Combining Equation 3.2, Equation 3.4 and Equation 3.5 results in the radar equation, Equation 3.6. By filling in typical values for the quantities a ratio between the transmitted power and received power can be found.

$$P_{received} = \frac{P_{transmitted}}{(4\pi)^3 \cdot R^4} \cdot \sigma \cdot G^2 \cdot \lambda^2 \tag{3.6}$$

**Transmission link**

To calculate the received power in case of a free space transmission link, the transmitted power density must be calculated first as well. This is the same as the transmission of the radar based system in Equation 3.1. The marker can be modelled as an antenna that receives power and then retransmits the power. The received power at the marker is calculated by multiplying the power density by the its effective area, which is done in Equation 3.7.

$$P_{received,tag} = A_{e,tag} \cdot G_{antenna} \cdot \frac{P_{transmitted}}{4\pi \cdot R^2} \tag{3.7}$$

This retransmission is the same as the initial transmission and can be calculated using Equation 3.1 as well. The received power is again calculated by multiplying the power density with the effective area of the antenna. However, the antenna gain is known for the receiving antenna and Equation 3.5 can be substituted in order to get the Friis transmission equation for a double antenna link, see Equation 3.8.

$$P_{received,antenna} = \frac{P_{transmitted}}{(4\pi)^3 \cdot R^4} \cdot A_{e,tag} \cdot G^2_{antenna} \cdot \lambda^2 \tag{3.8}$$

### 3.4.2. Reflections

The environment in which the tags need to be detected is the dry riverbed of the Río Colorado in Bolivia. This riverbed mainly consists of dry sand, with grain sizes in the range of 0.1 - 0.4 mm [9]. The tags are on or slightly below the surface of the sand and the antennas can be close above this surface. On the boundary between these media with different electromagnetic properties is a difference in impedance. This difference will cause reflections when a wave hits the boundary. The amount of power reflected can be indicated using the reflection coefficient. The reflection coefficient can be calculated using the difference in impedance of the media with Equation 3.9.

For a normal incidence wave on a boundary between two low loss dielectrics, with $\mu_0 \approx \mu_1 \approx \mu_2$ the formula for the reflection coefficient can be rewritten using only the relative permittivity $\epsilon_r$.

$$r = \frac{\eta_2 - \eta_1}{\eta_2 + \eta_1} = \frac{\sqrt{\frac{\mu_2}{\epsilon_2}} - \sqrt{\frac{\mu_1}{\epsilon_1}}}{\sqrt{\frac{\mu_2}{\epsilon_2}} + \sqrt{\frac{\mu_1}{\epsilon_1}}} = \frac{\sqrt{\epsilon_1} - \sqrt{\epsilon_2}}{\sqrt{\epsilon_1} + \sqrt{\epsilon_2}} = \frac{\sqrt{\epsilon_{air}} - \sqrt{\epsilon_{sand}}}{\sqrt{\epsilon_{air}} + \sqrt{\epsilon_{sand}}} \tag{3.9}$$

The permittivities for sand and air are listed in Table 3.1. Both media are nonmagnetic, meaning that their $\mu = \mu_0$. Finally, both media can be approximated as lossless: dry sand has a skin depth of several meters [16].

The reflected power is proportional to the square of the reflection coefficient $r$ and can be calculated using Equation 3.10 with the data from above. The reflected power due to the boundary between air and sand is 5.5%.

$$R = |r|^2 = \left| \frac{\sqrt{\epsilon_{air}} - \sqrt{\epsilon_{sand}}}{\sqrt{\epsilon_{air}} + \sqrt{\epsilon_{sand}}} \right|^2 = \left| \frac{\sqrt{1} - \sqrt{2.6}}{\sqrt{1} + \sqrt{2.6}} \right|^2 = 0.055 = -12.6 \text{ dB} \tag{3.10}$$

Table 3.1: Electromagnetic characteristics of air and sand [16]

| | **Relative permittivity $\epsilon_r$** | **Relative permeability $\mu_r$** |
|---|---|---|
| **Air** | 1 | 1 |
| **Sand** | 2.6 | 1 |

#### Clutter

Besides the interface between the air and the sand, there will also be small air pockets within the sand. Therefore, the sand is a non-uniform medium. When these pockets are sized in the same order or larger compared to the wavelength, these will cause reflections as well. Multiple received reflections are called clutter. In a lab setup, the clutter is constant and can be calibrated out by making an initial reference measurement [17]. However, when driving around, this clutter is far from constant and this method can not be used.

Exactly calculating the effects of clutter is difficult, because the plane wave approximation cannot be used when the reflective surface is small and the structure of the sand in the river is not known.

Part of the clutter can be eliminated. This elimination is implementation dependent. A variety of solutions is described below.

Implementations that use an impulse response can eliminate clutter in the time domain. For example, undesired clutter further away from the tags are irrelevant and can be discarded by windowing the time domain signal. Since the undesired reflections travel a longer distance, by windowing the signal in time domain these reflections can be filtered away.

Tags can also use frequency domain separation to remove part of the clutter as well. An electronic marker that is based on a re-transmission of a signal can retransmit the signal in another frequency band. By adding a filter to the receiver, most clutter can be filtered out.

The clutter can also be eliminated by depolarisation. Many surfaces do not change the polarisation characteristics of an EM wave, which can be utilised to distinguish between reflections and tags. This solution obligates tags that are able to change the polarisation of the retransmitted waves in comparison to the incident waves. If the transmit and receive antenna are cross-polarised and have a good polarisation isolation, many reflections will not be received. A disadvantage of this is the loss in power when the polarisation is randomised.

### 3.4.3. Noise

The detection system contains various noise sources. An ideal antenna does not generate noise, it only receives noise from the environment. In the environment of the antenna are natural noise sources and man-made noise sources. For this project, the antenna should receive signals from the ground, therefore it is directed at the ground. However, the antennas are not perfectly directional and noise from other areas such as the sky are received too. The largest natural noise source in the sky is the thermal noise from the sun. Man-made noise sources are electromagnetic influences from nearby radiation sources. One example might be the ignition system of a petrol car [18], on which the antennas might get mounted. The noise that naturally occurs is thermal noise from objects in the antenna path. In this section, these naturally occurring noise contributions are calculated.

For the noise calculations, the antenna is considered to be directed to the ground with the sun exactly above it. These values are realistic for antennas with an opening angle of about 60 degrees. The main lobe, the direction in which the most power is emitted, is directed to the ground while the oppositely directed back lobe is directed to the sun. For the calculations it is assumed that the antenna gain of the main lobe is 2 and the back lobe 1.

The antenna opening aperture directed to the sun is approximately half a degree, as shown in Equation 3.11. The antenna gain at this angle can be considered constant and is equal to the back lobe gain.

$$\Theta_{sun} = 2 \cdot \arctan\left(\frac{R_\odot}{r_\oplus}\right) \approx 0.5^\circ \tag{3.11}$$

From this data, the noise temperature can be calculated using Equation 3.12.

$$T = \frac{1}{4\pi}\int_0^{2\pi}\int_0^{\pi} R(\theta,\phi)\,T(\theta,\phi)\sin(\theta)\,\mathrm{d}\theta\,\mathrm{d}\phi = \frac{1}{4\pi}\Big(2\pi\cdot 2\cdot T_{ground} + (1-\cos(\Theta_{sun}))\cdot T_{sun}\Big) \tag{3.12}$$

Since the localisation of the tags is not during summer, with a cooler climate in the target area [9], a ground temperature of 300 Kelvin was chosen. For the sun temperature, $10^5$ K was chosen, which is an approximate long-term average for the sun temperature measured at 2.8 GHz [19]. Substituting the information in Equation 3.12 results in Equation 3.13.

$$T = \frac{1}{4\pi}\left(2\pi\cdot 2\cdot 300 + \left(1-\cos\left(\frac{0.5\pi}{180}\right)\right)\cdot 10^5\right) = 300 + 3.8 = 303.8\ \mathrm{K} \tag{3.13}$$

In Equation 3.13 can be seen that the noise from the ground has by far the largest noise contribution, and therefore the other natural noise sources can be neglected. With this temperature, the total noise power in the complete UWB-band from approximately 3 GHz to 10 GHz is calculated in Equation 3.14.

$$P_{noise} = k_b \cdot T \cdot B = k_b \cdot 300 \cdot 7{\cdot}10^9 = 2.9{\cdot}10^{-11}\ \mathrm{W} = -75\ \mathrm{dBm} \tag{3.14}$$

## 3.5. RFID implementations

This section will describe different implementations of RFID systems that could be used. For each design, the working principle, a possible realisation, the expected performance and its feasibility for assisting sediment research will be discussed.

### 3.5.1. Regular chipped RFID

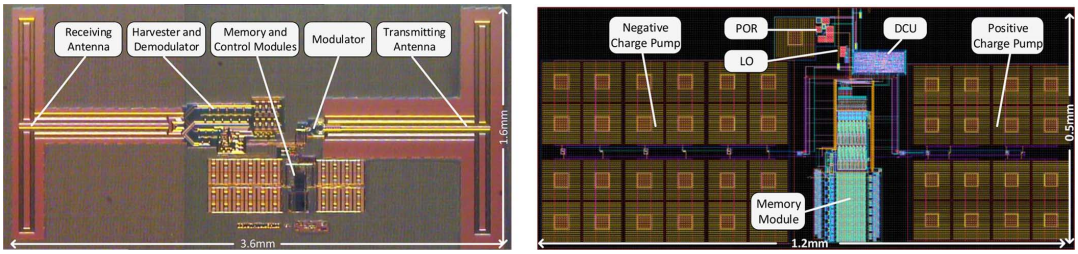


Figure 3.1: One of the smallest chipped tags designed [20]

Very small chipped RFID tags have already been designed [20, 21] one of them is depicted in Figure 3.1. Both of these were made by using an antenna that was directly embedded on the silicon die. The disadvantage of this is that silicon is a semiconductor and thus has quite a lot of loss. These tags also tend to use impedance modulation of the antenna which will only function as a method of information transmission in the near field. These effects combined make that these tags have a short reading range [20, 21]. Producing the tags for testing is also a challenge as advanced silicon processing is needed. Tags like the one depicted in Figure 3.2, which already have been used for sediment research such as in [6], are too large for this research and also have a limited reading range.

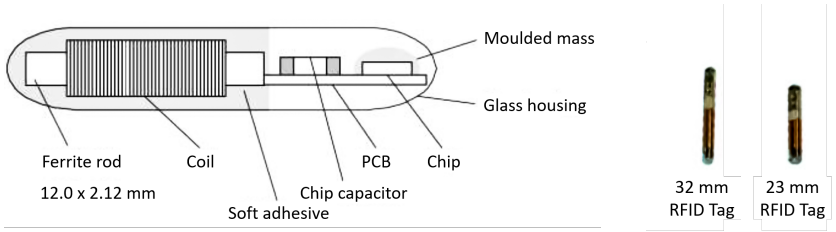


(a) Schematic drawing of the tag

(b) Picture of the tag

Figure 3.2: A tag previously used in sediment research [6]

### 3.5.2. Radar reflector

A radar or corner reflector is already commonly used to make ships and buoys easier to see on radar systems. These reflectors only have a diameter of 30 cm, but still significantly increase the radar detectability of a yacht.

Figure 3.3 shows the structure that the radar reflectors are based on. Incoming waves enter one of the octants and are reflected three times off the three perpendicular surfaces, which reverses the direction of the wave back towards the transmitter, parallel to the incoming wave. This allows for the very high RCS of these structures relative to their size.

The reflectors will need to be encapsulated in a material that is penetrable for a specific frequency band and impervious to all other frequencies for them to be uniquely identifiable. This way, the other frequencies are scattered in all directions but the single band is reflected back to the receiver with a high gain.

For this implementation, the difficulty is in the encapsulation material as there are no materials available with a high enough quality factor for their filter characteristics [22].

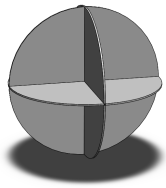

Figure 3.3: Render of the geometric structure of a radar reflector

### 3.5.3. Resonating Structure

A tag that is made of a resonating structure is an example of a passive, chipless, frequency coded design that has been discussed in section 3.3. Its main working principle is that an incident signal, often in the UWB-band, causes the tag to resonate on a certain frequency, similar to a tuning fork. This frequency response is then measurable at the receiving antenna.

A simple implementation is the use of microstrip dipoles with different lengths on a substrate as visble in Figure 3.4a [23]. The dipoles act as half-wave resonators, reradiating signals at different frequencies when incidented with a broadband pulse. By adding or leaving out one of the dipoles, bits can be encoded through the presence or absence of dips in the frequency domain. How this looks like can be seen in Figure 3.4b. For this particular implementation, five bits can be reached with five dipoles on a surface of $25 \times 30$ millimetres. The frequency range is between 5 to 6 GHz. One bit per 100 MHz bandwidth could be reached. When a 500 mW signal is transmitted, the maximum distance measured shows to be several tens of centimetres [24].

The main advantage of this tag is that it is extremely easy to make. They do not have to draw power from a battery and no semiconductor processes are involved. The drawback is that the range is restricted due to the limited amount of power that is radiated back.

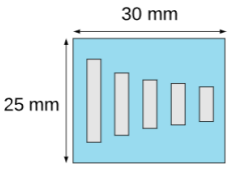


(a) The tag using dipoles of different lengths.

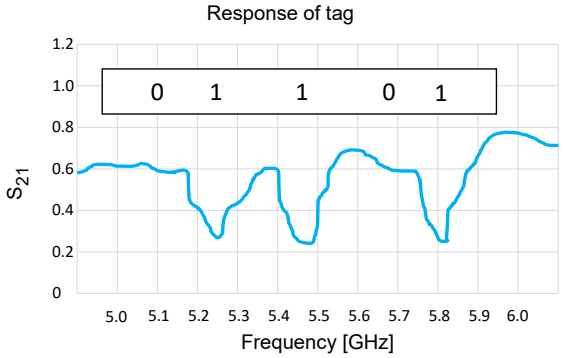


(b) Example $S_{21}$ response of the tag. A dip in the frequency indicates the presence of a dipole with a certain resonance frequency.

Figure 3.4: Frequency encoded tag as described in [23].

### 3.5.4. Transmission Line Delay

As was discussed in the previous section, a chipless tag can also be encoded using the time domain. This is done by adding parasitic elements on a transmission line, resulting in a specific sequence of returning signals. An example of such a system is described in [25]. This particular design is visualised in Figure 3.5a and its lumped element model in Figure 3.5b. Evenly distributed capacitors along the line create impedance mismatches in the transmission line which create reflections. Placing or not placing a capacitor will create the possibility to encode one bit.

The tag in question has four bits on a board of $82 \times 31$ millimetres. The tag operates in the UWB frequency range and its maximum reading distance is calculated to be 56 centimetres.

A big disadvantage of these tags is their size. Each segment between a capacitor has to be at least 18 centimetres long to avoid temporal overlap. This makes miniaturisation very difficult. Its advantages are that the tag design is very simple and predictable, which makes it cheap and easy to design.

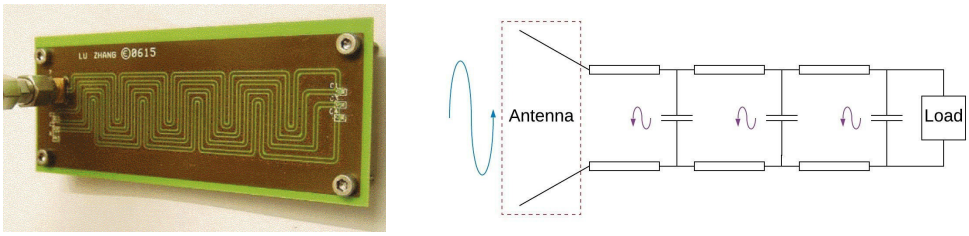


(a) A time encoded tag, as described in [25] (b) A lumped element model of a time encoded RFID tag

Figure 3.5: Time encoded RFID tags

### 3.5.5. Non-linear tag

As described in subsection 3.4.2, clutter can be significant when measuring UWB pulse responses. This will quickly cause the tag response to be buried in this background clutter. A solution is to have a tag that will contain a non-linear element in it that will create harmonics of the incoming signal [26]. These harmonics can still effectively be transmitted by the tag's antenna as the new wavelength will be a unit fraction of the old wavelength. The advantage of this frequency shift is that now the clutter is in a different frequency band than the tag response. This allows for the clutter to simply be filtered out and only the received noise matters as described in subsection 3.4.2.

These tags can be realised with a straight dipole antenna connected to a diode, but this will make them half as large as the wavelength of the used radio frequency. To keep the tags small, folded dipole structures can be considered, but these are more difficult to optimise and can still only be reduced in size 5 times as described in subsection 3.6.1. Figure 3.6 shows a folded dipole implementation.

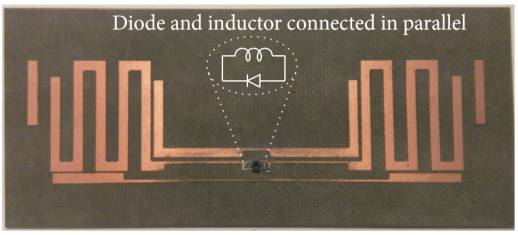


Figure 3.6: Folded dipole structure with a non-linear element as discussed in [26]

## 3.6. RFID antenna miniaturisation techniques

When a chipped tag is designed, the main part of the tag size is determined by the antenna. The size of an antenna design is mostly related to the wavelength it is tuned to. By folding the antenna, the size can be reduced to about a fifth of the wavelength [27]. For a 4 mm tag this would correspond to a tuning frequency of about 15 GHz, and such high frequencies would dramatically increase the amount of clutter coming back from the surface and no commercial RFID chips would be available for use.

### 3.6.1. High permeability magnetic core antenna

Another way to miniaturise antennas is to increase their effective aperture by using ferromagnetic (high permeability) materials [28]. This is a practice commonly found in long- to shortwave radios and more recently in low frequency RFID applications [6]. The reactive energy stored in the magnetic material might be used to create a separation in time or frequency domain between the received signal and surface clutter. Current designs using this technique are much larger than the maximum specification in this project, see Figure 3.2. These tags also mostly operate in the near field and thus have a small reading range.

### 3.6.2. High electric permittivity materials

Another method to shrink antennas and resonators is to embed them in a high permittivity material. This is somewhat similar to using magnetic materials. The shorter wavelength in a high dielectric material makes it possible to shrink a given conductive structure while maintaining the same tuning frequency. A practise commonly used in mobile phone antennas [29], an example is shown 3.7.

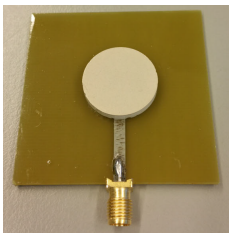

Figure 3.7: Ceramic high permittivity antenna [30]

## 3.7. Choice of implementation

The designs discussed in section 3.5 are compared and evaluated in Table 3.2. After careful consideration, it was chosen to implement the system described in subsection 3.5.3. This is a chipless frequency encoded tag, which has a frequency dependent radar cross section. This method was chosen as it is easy to produce and prototype, has the potential to be created at the required sizes [31] and promises an adequate reading range [32].

Based on this design choice a system overview was created. This is visualised in Figure 3.8. For the sake of this project, this system was divided into three subsystems. For each subsystem a thesis is written. The system consists of the tag, transceiver hardware and signal processing. A detailed report on the tag design is written by [33]. In [10], the design of the transceiver hardware will be described. This mainly consists of the design of antennas. Measuring data is one thing, but interpreting is at least just as important. In [11], the signal processing system will be designed.

For the entire system, a preliminary calculation on reading distance was made using Equation 3.6. The worst case was assumed, given a frequency of seven gigahertz. The gain of the antennas was set to one, and a radar cross section $\sigma_{RCS}$ of -60 decibel square meters. The transmitted power was set to be 32 Watt, and the power received -110 dBW. The maximum reading range was then derived to be 1.3 meters using Equation 3.15 from [32].

$$R = \sqrt{\frac{P_{tx,max} G_{tx} G_{rx} \lambda^2}{P_{rx} (4\pi)^3} \sigma} \tag{3.15}$$

Table 3.2: Implementation consideration table

| | Bit density | Ease of manufacturing | Clutter sensitivity | Material availability | Power requirement |
|---|---|---|---|---|---|
| **Chipped RFID** | + | - | ++ | + | - |
| **Radar reflector** | 0 | + | + | - - | + |
| **Resonating structure** | 0 | ++ | 0 | 0 | 0 |
| **Transmission line delay** | - | - | 0 | + | - |
| **Non-linear tag** | - | 0 | + | + | - |

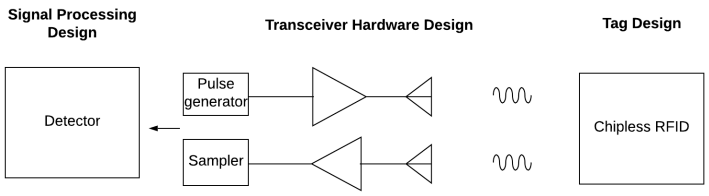


Figure 3.8: Overview of the system divided into three parts.

# 4

# RFID Tag Design

As is discussed in the system design, the design will be based on passive, chipless RFID tags that are encoded in the frequency domain. This type of tags uses the natural resonance of the antenna structure as its identification. This technique relies on the inherent information incorporated in the tag's structure [34]. These tags give a high reliability in rough circumstances and leave the possibility to miniaturise to very small structures [13].

In this chapter, the design of the tag will be further elaborated on. First, a short recap on the types of chipless designs will be given, and why it was chosen to focus on frequency coded designs. Then, a technical programme of requirements for the tag is set up. Subsequently, important characteristics of frequency coded tags will be explained. After this, four possible designs will be discussed, of which one will be chosen. This design will then be further discussed in detail.

## 4.1. Types of chipless designs

As was discussed in the previous chapter, chipless tags are often categorized into two types [15]. In the first category, data is encoded by positioning parasitic elements along a transmission line to create reflections at precise moments.

In the second type, the antenna is a resonating element which causes peaks (or dips) in the frequency spectrum of the reflected signal. Temporal coded tags often have longer reading ranges than spectrum coded tags. The spectrum coded tags use high frequencies, which limits their range. However, spectrum coded tags have higher information densities, which allow them to reach smaller sizes for the same information stored.

It was concluded that frequency domain coded tags should be used, since their information density is higher, which allows for smaller sizes with the same information stored.

## 4.2. Programme of requirements

Although a programme of requirements was made for the entire system in chapter 2, a more specific one should be made for the design of the tag. This programme of requirements will help to set boundaries for the design that this thesis is build around.

In order to set the requirements on the size of the tag correctly, it is important to have a size categorisation for sediment. If these categorisations are set, one can scientifically say if the tag reaches the size of sand grains. For this, a paper by Wentworth in the Journal of Geology is used [35]. According to Wentworth, the biggest sand grains are *very course sand grains*, which are in between 1 and 2 millimeter in diameter. Above this size, between 2 and 4 millimeters, one speaks about *granule gravel*. Using this terminology, a requirement table was set up. Some of the system requirements overlap with the tag's requirements, because these were already related to the tag. Each requirement was also ranked on priority. This made it clear in what direction trade-offs needed to be made.

| Nr. | Product Requirement | Priority |
|---|---|---|
| PR1 | The tracers should be uniquely identifiable up to a 100 devices | High |
| PR2 | The tracers should be able to reach the size of *very course sand grains* or *granule gravel* (1 to 4 millimeters) | High |
| PR3 | The tracers should be detected wirelessly | High |
| PR4 | The tracers should have a range of 40 centimeters | Medium |
| PR5 | The tracers should still be detectable up till 5 centimeters in sand | Medium |
| PR6 | The tracers should be detectable from a vehicle | Low |

Table 4.1: The RFID tag's technical requirement table

## 4.3. Important characteristics

To understand the working mechanisms of chipless tags, some important characteristics need to be understood. In this section, the Radar Cross Section (RCS), the quality factor and the damping factor will be discussed.

### 4.3.1. Radar cross section

When an electromagnetic wave is incident on a chipless tag, it sends some of the energy to different directions. This is called *scattering* [24]. If the transmitting and receiving antenna are very close to each other, or even overlap, the direction of the incident wave is the same as the direction of observation. This phenomenon is called *backscattering*.

It is often very difficult to describe the fields around an RFID tag. That is why researches often describe the characteristics of the resonance with a fictitious surface: the Radar Cross Section [36]. The RCS is a measure of how detectable an object is by a radar. It does not necessarily correlate with the physical surface of an RFID tag. Typical values of a radar cross section are set out in Table 4.2 [24][37].

Table 4.2: Typical RCS Values [24][37]

| Target | RCS ($m^2$) |
|---|---|
| Bug | $10^{-5}$ |
| Small Bird | $10^{-2}$ |
| Man | 1 |
| Large commercial airplane | 100 |
| Resonance based chipless RFID tag | $3 * 10^{-4}$ |

The RCS relates the power density measured at the tag with the power density at the receiving antenna. The captured power $P$, the incident power $W_i$ and scattered power density $W_s$ relate according to the relationships in Equation 4.1 and 4.2 [24]. Equation 4.2 implies isotropic scattering. The functional system is depicted in Figure 4.1 and the equations related to an entire RFID system can be found back in subsection 3.4.1

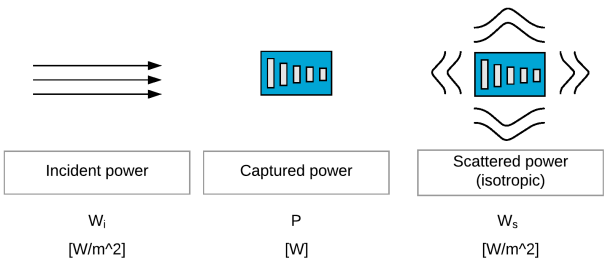


Figure 4.1: Operation of an RCS based chipless tag. The related equations are Equation 4.1 and 4.2

$$P = \sigma_{RCS} \cdot W_i \quad \text{(W)} \tag{4.1}$$

$$W_s = \frac{\sigma_{RCS} \cdot W_i}{4\pi R^2} \quad (\text{W m}^{-2}) \tag{4.2}$$

### 4.3.2. Quality factor

As was said in the beginning of this chapter, the quality factor is very important in case of scattering RFID tags. A high quality factor means that the tag is very frequency selective. This means that the tag is detectable by it's high and narrow peaks.

The quality factor can be described as a measure of the losses in a resonant circuit. The lower the losses, the better the circuit resonates, and the better the Q factor is. The losses of a resonating circuit can be divided into three types: radiation losses, dielectric losses and conduction losses. In the case of a resonating structure, radiating losses are desired, since these are the losses that are aimed to be measured. The other two loss sources are undesirable and can impact the detectability of a tag a lot. Tags that are printed on low cost substrates like paper can have significant dielectric losses [24]. In this case the overall quality factor is dominated by the dielectric losses of the substrate, and not by radiation.

### 4.3.3. Damping ratio

The damping ratio or damping factor is a dimensionless system parameter that describes how fast oscillations in a circuit decay after a disturbance. It is also often used in relation to resonating structures and inversely related to the quality factor by Equation 4.3.

$$\zeta = \frac{1}{2Q_0} = \frac{\alpha}{\omega_0} \tag{4.3}$$

## 4.4. Possible designs

Based on the previous design choices, four possible designs were chosen. In this section, these four designs will be discussed shortly and compared with each other. Finally, one of these designs is chosen to be proceeded with. This is the design that will be used in the prototype and that will be extensively simulated.

### 4.4.1. Quarter-wavelength slot resonators

A circular shaped tag with an optimised coding capacity was proposed in the beginning of 2014 [38]. The structure of the tag can be seen in Figure 4.2. 24 notches of different sizes are integrated. Each notch behaves as a quarter wave resonator, causing a dip in the tag's signature. By short circuiting a notch, it is possible to eliminate one resonant dip. This allows for a 24-bit resonator on a 24 by 24 milimeter surface. This gives a coding density of 4.1 bits per $cm^2$. This is relatively high.

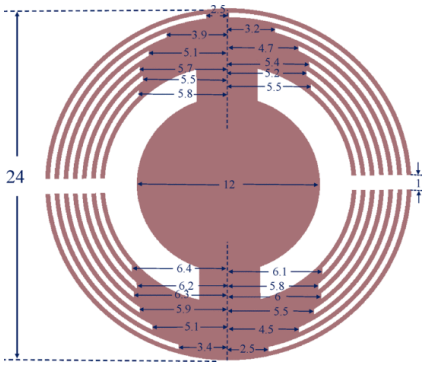


Figure 4.2: A 24-bit chipless RFID tag based on quarter wavelength slot resonators [38].

Another interesting finding of this tag's research was its relationship between the dielectric permittivity of its substrate, its damping and its resonance frequency [34]. As can be observed in Figure 4.3 and 4.4, the higher the dielectric permittivity of the substrate the structure is printed on, the lower its damping factor and resonance frequency. When the dielectric permittivity of the substrate is between 2 and 3, the damping factor of the tag increases. In this region, the resonant frequency of the tags are close to the resonant frequency of the metal, which causes damping to occur [34].

The tag's directivity was also measured, showing quite a lot of sensitivity to the incident angle of the transmitted signal. This is not desirable in the application of this thesis, since tags will have a random orientation upon tracking in the riverbed [38].

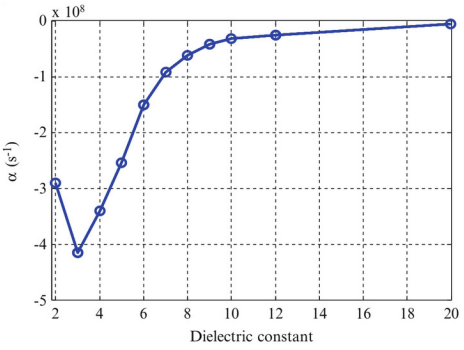


Figure 4.3: Damping factor of the circular tag at its resonant frequency versus dielectric constant of its substrate [34].

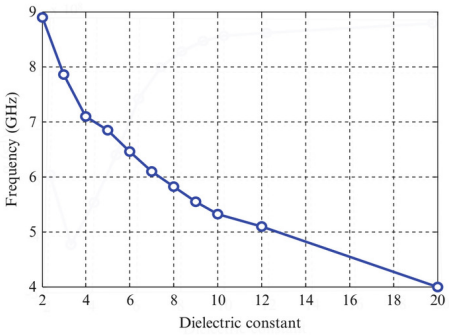


Figure 4.4: Resonant frequency of the tag versus the dielectric constant of its substrate [34].

### 4.4.2. Capacitively-tuned microstrip resonators

This implementation has already been discussed in subsection 3.5.3 [23]. The design is based on the use of grounded microstrip dipoles with different lengths on a substrate. Every dipole acts as a half-wave resonator, with a different resonating frequency due to differences in length. By adding or removing the strips, bits are coded into the tag.

In this paper, five bits were reached with five dipoles on a surface of 25 by 30 milimeters which amounts to a density of 0.67 bits per square centimeter. The structure was printed on a low-loss substrate with a dielectric permittivity of 2.2. The frequency range of the resonating dipoles is between 5 to 6 GHz. One bit per 100 MHz could be reached without overlap in detection. When a 500 mW signal is transmitted towards the tag, the maximum distance measured shows to be several tens of centimeters [24].

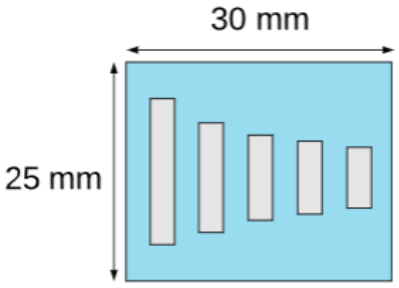


Figure 4.5: A 5-bit chipless RFID tag based on capacitively-tuned microstrip resonators.

### 4.4.3. Miniaturised fragment loaded open loop resonators

This design is a result from a very recent paper that was published in 2018 by the University of Science and Technology of China [31]. This tag is based on a standard open loop resonator filled with fragments. The fragments influence the tag's resonant frequency and quality factor. The optimal fragment configuration is found using a evolutionary algorithm with genetic operators (MOEA/D-GO) [39].

The tags operate in single mode, which means that they resonate only at one frequency. This means that to create many different tags, different configurations have to be generated. A benefit of single mode operation is that the tags can reach very small sizes. Its coding densities can reach approximately 3.58 bits per resonator of 3.4 x 6.3 mm, which is equivalent to 16.7 bits per square centimeter. This appears to be the highest reached in literature for passive, chipless, frequency coded tags.

From a 30 centimeter distance in controlled conditions, the tag shows very clear Radio Cross Section peaks at its simulated resonant frequency. Its optimal tag shows a Quality factor of 131.8 and a resonant frequency at 2.9 gigahertz and is depicted in Figure 4.6.

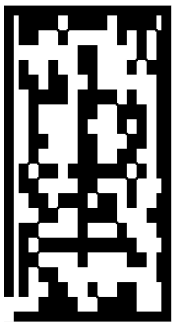

Figure 4.6: Fragmented Open-Loop Resonator with a Quality factor of 131.8 and a resonant frequency of 2.9 gigahertz [39].

### 4.4.4. Planar filter tags

One of the first passive, chipless, frequency coded designs that has ever been studied in detail makes use of two wideband antennas connected with a microstrip line [40] (see Figure 4.7). Along the linked line, spiral resonators of different lengths are positioned. These resonators will create dips in the tag's spectral response, which is measurable.

Groundbreaking in this design was that it was the first design of this type to ever reach the coding density of a European standard optical barcode [24]. The final design. After optimization of the structure (by meandering the microstrip and placing resonators on both sides), the design was able to reach a total capacity of 35 bits on a 88 by 65 milimeter surface. This is 0.61 bits per $cm^2$. The tag operates in the ultra wide band from 3 to 7 GHz.

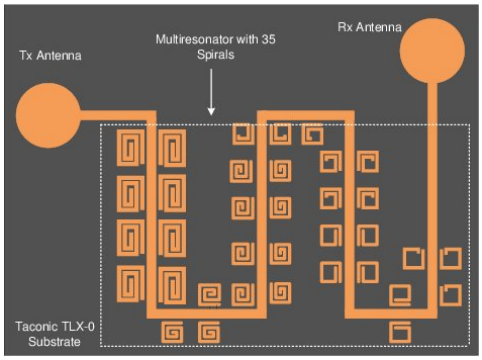


Figure 4.7: Two wideband antennas connected by a meandering microstrip with resonators on both sides [41].

### 4.4.5. Chosen Design

After analyzing these four designs, a choice had to be made. Time and resources did not allow to make all four of the tags. Moreover, not all tags are seem to be scalable to the size of a sand grain.

It was clear that the planar filter tags would be difficult to scale down, since a transmitting and receiving antenna are always integrated in the design. For this exact reason, the coding density of the design has stayed under the one bit per square centimeter. One could try to make a design with only one antenna, but this would also not result in the required size. The tag based on capacitively-tuned microstrip resonators has a very similar coding density to the planar filter tag. the tag can be sized in one dimension, by changing its operation to single mode. This means tat only one dipole would be used, and tags would be distinguishable by its resonant frequency. There is however, one limitation. Since the resonators act like half-wave dipoles, the length of such a resonator would be 1.5 centimeters at 10 gigahertz, as can be seen in Equation 4.4. This size is not close enough to the size of a sand grain. Frequencies in this range also cause way too much clutter.

$$\frac{\lambda}{2} = \frac{c}{2 \cdot f_0} = \frac{3 \cdot 10^8}{20 \cdot 10^9} = 0.015 \quad \text{(m)} \quad (4.4)$$

The quarter wavelength slot resonator has a high coding density, but its current design is yet too large for the requirements in this thesis. Just like the resonating dipole tag, one could size by stripping off layers from the structure. The tag would then operate with less bits, but one could still distinguish the tags by placing the resonant frequencies differently. Another option would be to still look at linear scaling the tag. To reach the size required in section 4.2 , we have to at least scale the tag down by a factor of six. Since the tag already functions in the ultra wide band, it will most likely have too high resonant frequencies.

When it is considered that the tag should be scalable to the size of a sand grain, the fragmented open loop resonator seems to be the best option. The tags described in the research paper are the closest to reaching a submillimeter size. With smaller structures, the algorithm might still be able to create a structure with a resonant frequency in the ultra-wideband and a reasonable quality factor.

## 4.5. Fragmented open loop resonators

As it was chosen to design the fragmented open loop resonators described in subsection 4.4.3, this design will be further elaborated on. First, the performance of open loop resonators in general will be discussed. After this, the concept of fragment loading is explained. Then, the final architecture of the tag is laid out. Finally, it is explained how the optimal fragment configuration is obtained and how this is used to design even smaller tags than is mentioned in the paper.

### 4.5.1. Open loop resonators

Open-loop resonators have been used in the design of bandpass filters [42]. At resonance, an open-loop resonator has its maximum electric field density at the side on which the gap is open, and its maximum magnetic field density exactly at its opposite side. Since 2014, the use of open-loop resonators for chipless RFID applications have been explored [43]. Since then, novel ways of configuring the resonators for higher coding densities and better performance have been found [44]. One of these tags also used the cross-polarisation characteristics of the open loop resonators [45].

### 4.5.2. Fragment loading

One of the biggest challenges with designing chipless RFID tags based on open-loop resonators is to use space efficiently, which further miniaturises the design. It was found that fragment loaded structures gave great flexibility in shaping a structure with good performance [46, 47]. The benefits of using fragment loading have been proven in several occasions, where antenna and microstrip components reached a performance superior to designs with orthodox structures.

### 4.5.3. Tag architecture

The fragmented core and open-loop resonator combined finally amounts in an architecture in Figure 4.8. The fragmented core is shifted by 0.1 milimeter, leaving a small gap at one side of the core. This distance $d$ can be used to fine-tune the design [31]. The width $w$ of the open loop walls is set to be the same as the width of one patch.

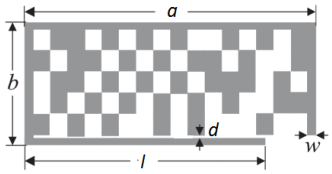


Figure 4.8: Representation of the tag (redesigned from [31]).

### 4.5.4. Optimisation

The central idea behind fragment loaded tags is that they are not based on known structures as these do not guarantee the best performance for a given size. To find structures that can function as a tag, the space of all possible fragment configurations must be searched. The requirements on the fine size of the fragments makes that the number of possibilities becomes too large to simply traverse all points in this search space. This problem is worsened by the time it takes to evaluate a single design as this can only be done using EM simulations. Thus an efficient multi-objective optimisation function is needed to find the best configurations within a workable amount of time.

The open loop architecture can be optimised following the method that is brought forward in the original paper that proposes this design [31]. The implementation is based on a Multiobjective Evolutionary Algorithm based on Decomposition combined with Enhanced Genetic Operators (MOEA/D-GO algorithm). The original source code used by the researchers was not made available. By combining the information given in the paper with the original sources for the algorithm [48] [39], an implementation was constructed. The base implementation of the MOEA/D algorithm was available as an open source collection of MATLAB files [49]. This codebase was then adapted to work with MOEA/D-GO using a linear summation decomposition.

The algorithm is based on the evolutionary theories of Charles Darwin starts by generating a random population of tags. This population has a specified size [50]. Then, generations of tags will be iterated, by randomly mutating tags, crossing them over with each other and introducing new random structures to the population. For every generation, the most optimal tags are chosen and move on to the next generation.

In order to optimize the tags for certain objectives, the cost function was specified. The cost function generates the tag model based on the position of the currently evaluated individual in the search space (see Equation 4.5). Next, the function invokes an HFSS script. The HFSS script imports the generated tag model to the simulation environment, assigns the copper material to the tag, converts the generated vector model to a solid and will then execute the simulation over a range of frequencies. After the simulations are done, the script exports the average bistatic RCS over frequency in cross polar orientation as depolarising tags can help with filtering out clutter. The HFSS script removes the tag model to restore the environment to the initial state and closes the program. The simulation data will now be used to derive the cost factors for the tag. The algorithm will then use these cost factors to evaluate the performance of an individual tag. The output of the algorithm is an estimated Pareto front. A Pareto front describes all points in the search space of which the performance can not be increased by moving in a single direction. After numerous iterations of the algorithm, the estimated Pareto front will approach the actual front. All adapted and new scripts can be found in Appendix A. A very general overview of the algorithm design is visualized in Figure 4.9.

The multi-objective optimisation problem or cost function can be described as follows:

$$\begin{aligned} &\min\ F(x) = (f_1(x), f_2(x), ..., f_n(x)) \\ &s.t\, x \in \Omega \end{aligned} \tag{4.5}$$

Where Ω is the decision space containing all possible tags and $x$ is a matrix containing only ones and zeroes describing the fragments in a tag. The equations below are the functions on which the tag will be evaluated.

$$f_1(x) = \max(|f - f_0|, 0) \tag{4.6}$$

$$f_2(x) = \max(|f_2 - f_p|, 0) \tag{4.7}$$

$$f_3(x) = \max((\frac{RCS[f]}{RCS[f-1]} + \frac{RCS[f]}{RCS[f+1]})/f_0, 0) \tag{4.8}$$

$$f_4(x) = max(|RCS| - |RCS_0|, 0) \tag{4.9}$$

$f$ is the resonant frequency of the current tag described by $x$, $f_0$ is the desired resonant frequency, $f_2$ is the frequency of the second resonant mode, $f_p$ describes the desired location of a second mode and $RCS$ the radar cross-section over frequency in dB square meters. The $RCS$ is derived for a given set of discrete frequencies and is thus treated as a sampled variable.

Equation 4.8 is used as an estimator for the quality factor of the tag, this was done this way because the eigenmode simulation type which can directly compute the cavity resonance, and thus Q, of a given structure did not give solutions that were consistent with the bistatic RCS simulations. An airbox had to be drawn around the structure that greatly influenced the outcomes of the simulations. In the eigenmode simulations, this airbox was not constant and this made simulations unreliable.

For the new tags, the simulations parameters shown in Table 4.3 were chosen. The maximum resonating frequency was not expected to surpass 8 GHz as the open loop has its resonant frequency around 7 GHz and the fragments tend to reduce this. The minimum frequency was chosen at 3 GHz as this is the lower limit for the UWB band. The target RCS is set at -30 dBsm as this is above what is attainable but it also reduces the dominance of the RCS factor in the optimisation problem. The base structure was chosen to be a 4 x 4 millimeter open loop. This size was chosen as it is the minimum requirement of the tag size, as is discussed in section 4.2. The length and width reach the maximum grain size of the smallest type of gravel [35].

This new base structure was first simulated without fragment loading to check if it would not compromise on performance compared to the original tag. Figure 4.11 shows a comparison between the original open loop tag and the new square base structure. The height of the peaks is comparable and the frequency still lies within the band of interest. The depolarising effect is also maintained so optimising tags based on a 4 by 4 millimeter loop are worthwhile to be optimised. The fragments are laid out in a 15 by 15 matrix. The slot on the left side is kept at 0.1 mm just as in the original structures. This slot is created by shifting all fragments to the right, this also creates smaller fragments on the other side of the tag which seems to be important as most solutions tend to leave a gap in the corner opposite the loop opening. More on how this will be generated into a Computer Aided Design (CAD) is explained in the next chapter.

Table 4.3: Parameters for the optimisation of the new tags

| $\mathbf{f_0}$ | $\mathbf{f_p}$ | $\mathbf{RCS_0}$ |
|---|---|---|
| 3 GHz | 8 GHz | -30 dBsm |

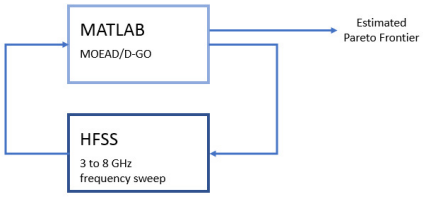


Figure 4.9: Schematic representation of the optimisation system

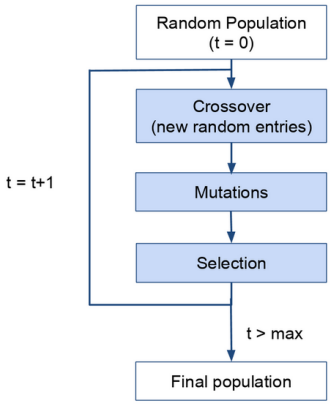


Figure 4.10: Schematic representation of the genetic algorithm

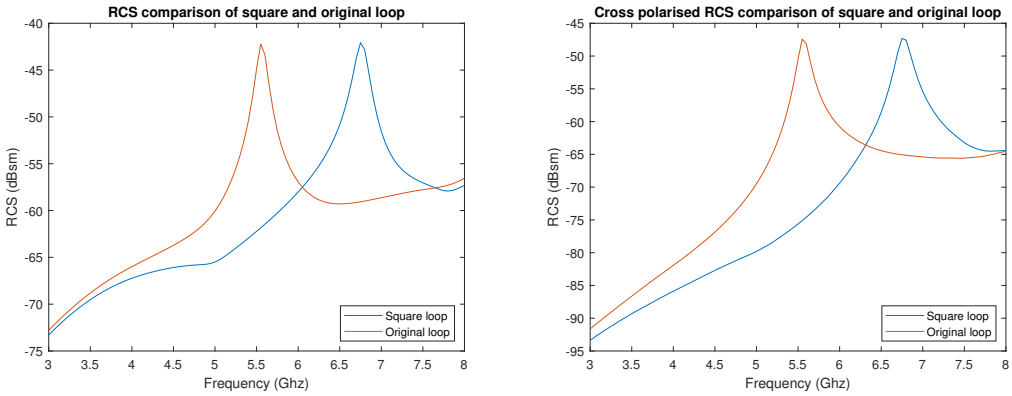


(a) (b)

Figure 4.11: Comparison between an open loop resonator of 4 by 4 millimeters and the original size (6.4 by 3.4 millimeters).

**Preliminary optimisation results**

After a few iterations of the algorithm, a few of the tags were extracted, the full population performance is availible in Appendix C. These might not be the best solutions available yet, but they do show desired behaviour. The tag shown in Figure 4.12a, will resonate at 4.425 GHz. The cross polarised RCS peak reaches a level of -69 dBsm, which is higher than the one reached by the best original tag found in [31]. Which shows that it might be worthwhile to investigate what would be the optimal base structure. The second example of the extracted tags resonates at 6.75 GHz at a cross-polarised RCS peak of -52 dBsm, which is again higher than the best reference tag. An interesting observation that can be made is that a lot of tags in the estimated Pareto front after eight iterations are similar. This might indicate that the mutation probability, now 1%, should be higher to maintain diversity. The relatively small diversity found does not have to be a problem, as multiple tags can be constructed from one solution by removing fragments [31]. The probability of finding the best solution however, does go down with smaller variation.

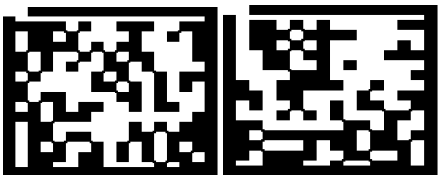

(a) (b)

Figure 4.12: Two examples of new optimised square resonators

# 5

# Simulation and Design Verification

To gather more information on the properties of the chosen tags, simulations have been run. These simulations were done using Ansoft HFSS [51]. This particular software is also used for the optimisation of the open loops so the same set of scripts is used to generate models of the tag. In this chapter, simulations of the design will be discussed. First, the simulation set-up is described. Then, it is described how a matrix of zeros and ones can be converted into a file that can be integrated in HFSS. Finally, simulations of the tags described in the paper and newly generated tags are examined.

## 5.1. Simulation set-up

The most important property to be verified is the RCS of the tag. It is also particularly important to report on the tag's directionality since the source of the design does not report on this, and the tag could lay in any random position on the riverbed. HFSS has built in functions for calculating a radar crossection. To construct the simulation environment for performing bistatic RCS simulations, Ansoft's documentation was consulted. The environment consists of the tag on an FR4 substrate, surrounded by an airbox. The airbox is then surrounded by a Perfectly Matched Layer (PML) to absorb the radiation, this is required as the simulation space is finite so a boundary condition needs to be set which simulates free space radiation. It is recommended by Ansys to keep this PML at least a quarter wavelength away from the tag.

In the constructed simulation space a plane wave excitation source is inserted as a means to model the tag being read. The plane wave excitation can be configured to have different incident angles. After the simulations are run for a discrete set of frequencies, the RCS is calculated by software over a range of reception angles.

## 5.2. Automated CAD design

In order to run the simulations, a matrix of zeros and ones needs to be converted into a three dimensional model of the RFID tag. The script that is used to do this can be found in Appendix A.

From the genetic algorithm, a binary matrix is created which present the fragments in the open loop resonator. The open loop is not yet included into the matrix. The first step is to expand the matrix. Each fragment is 0.2 by 0.3 millimeters [31]. By expanding the matrix by 3 in length and 2 in width, making every number a 0.1 by 0.1 millimeter block. This matrix will be placed within the open loop. Finally, the matrix is shifted 0.1 millimeter to the right, to create the gap indicated by $d$ in Figure 5.2.

## 5.3. Verification of the original tags

To expand on the knowledge about the proposed tags in [31] and to verify the correctness of the simulation environment, a reference tag was simulated. In the paper, little is said about the scattered directivity of the tags. After verifying the simulation environment, the directional behavior of the reference tag will be explored. The reference tag used is shown in Figure 4.6 and has a resonance frequency of 2.9 Ghz and a quality factor of 131.8.

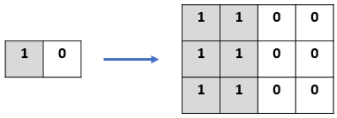


Figure 5.1: The principle of expanding the matrix to blocks of 0.1 by 0.1 millimeters

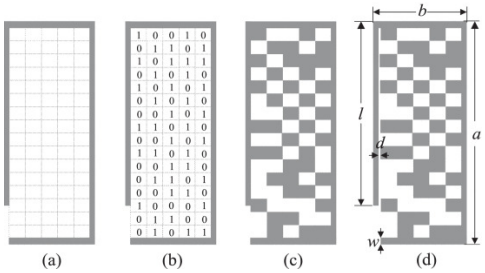


Figure 5.2: The principle of (a) placing a matrix in the open-loop resonator, (b) filling this matrix with a binary value, (c) adding a metal fragment for the 'ones' and (d) shifting the matrix by a length $d$ [31].

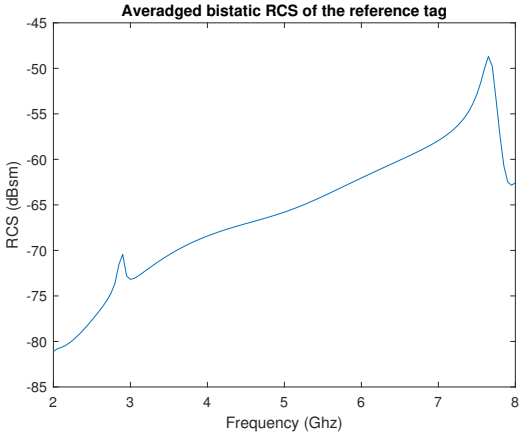


(a) RCS of reference tag

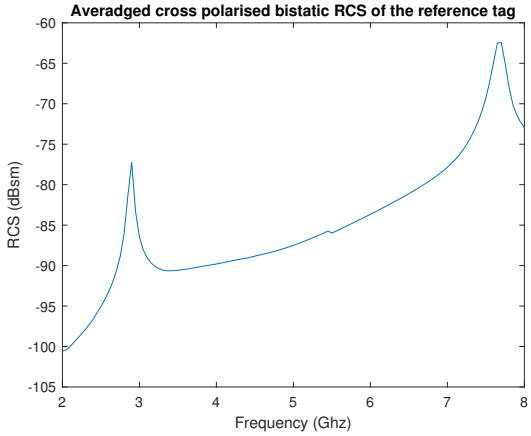


(b) Cross-polarised RCS of the reference tag

Figure 5.3: Simulated RCS values of the reference tag

### 5.3.1. Radar Cross Section

Figure 5.3 shows that the reference tag in Figure 4.6 indeed has a peak in its radar cross section characteristics, although it is lower than the 2.9 Gigahertz in the paper. This can be caused by a difference in the simulation setup and exported data. It can also be caused by a difference in substrate, as the tag was simulated on an FR-4 substrate. As was shown in Figure 4.4, the dielectric permittifivity can greatly influence the place of the resonance peak. Figure 5.3 shows an average RCS over all reception directions. The parameters used to obtain the figure shown in the paper are not known [31]. Figure 5.3(b) shows the RCS when simulated in a cross polarised setup. These results show that these tags are at least somewhat depolarising. Which can aid detection when filtering for clutter. The open loop tag data in Figure 4.11 also showed this depolarising behaviour. This gives an indication that most open loop tags will show this behaviour.

### 5.3.2. Directional behaviour

In the case of sediment research, the orientation of the tags on the riverbed will not be known. It therefore will be important that the tag does not exhibit a too directional radiation pattern. If the tags would only radiate in a certain direction this would likely cause a lot of failed detections. As was stated earlier, the directionality of fragment loaded open loop tags is currently not known so this required investigation. For this, the data from the previous RCS simulations can be used.

Figure D.2 shows the directional properties of the reference tag when simulating a co-polarised bistatic RCS measurement with the tag oriented along the XY-plane width the long side pointing along the Y-axis. The gap in the loop is oriented towards the positive Y-direction The tag is exited using a plane wave with the electric field oriented in the X-direction. Under these conditions, the tag shows a strong damping in the negative Y direction, indicating that it will radiate more efficiently in the direction where the gap is oriented. The RCS

is largest in the negative Z-direction, which would be very hard to detect if the antennas are pointing at the ground. Cross-polar directionality was also investigated, as detecting it this way will provide isolation from clutter. The resulting pattern is shown in Figure D.1, this measurement results in a much more even pattern than the co-polarised case. The response of the tag only vanishes around the YZ-plane. This is likely caused by the short side of the tag, which is in the same direction as the electric field polarisation of the plane wave. If the receive antenna can only see the short side, the response will be very small. This configuration also does not show the strong response on the bottom side, the best response would be achieved if the receive antenna would be slightly off-axis with respect to the transmitter. This could easily be realised while mounted on a moving detection system.

## 5.4. Properties of generated tags

To evaluate the newly generated tags, a simulation has been done on tag (a) of Figure 4.12. Tag (b) has not been simulated, since this would stagnate the optimization algorithm, which is still running as this thesis is submitted.

Figure 5.4 shows the simulated RCS of one of the tags generated by the algorithm, when comparing it to previous tags, a number of things stand out. Firstly the absolute value of the peak is higher than that of the reference tags. However, the peak does not stand out as much as for the reference and the Q-factor is only 25. It might be because the tags are optimised for cross-polarised RCS and this value -63 dBsm is higher than that of the reference tag in a cross-polar measurement. Another possible explanation for the low Q-factor is that the numerical value of the RCS dominates that of the Q estimation done by the algorithm.

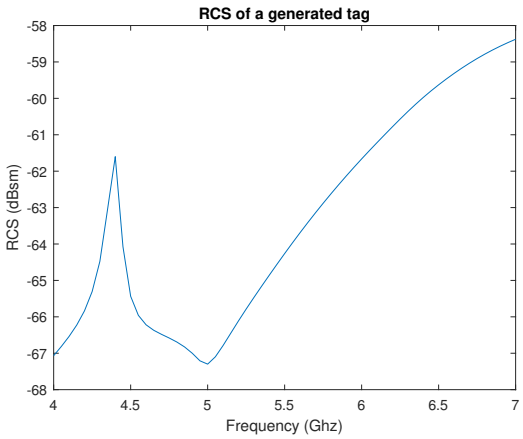


Figure 5.4: RCS of one of the generated tags

# 6

# Realization and Testing

To verify the simulations, designs from the research paper were ordered on standard Printed Circuit Board (PCB) material [31]. Subsequently, an attempt was made to characterize these tags in the Radar Laboratory at the faculty of Electrical Engineering, Mathematics and Computer Science at Delft University of Technology.

## 6.1. Design Factors

In the realization of the tags, several important design choices were made. In this Section, two of these design choices are explained and justified.

### 6.1.1. Substrate

In Section 4.3.2 and Subsection 4.4.1, the influence of the substrate on a tag's performance is already shortly discussed. As was seen in Figure 4.3 and 4.4, the dielectric permittivity of the substrate can greatly influence both the damping factor as the resonant frequency of the tag. Ideally, the tag has a low damping factor and a low resonant frequency. Lower resonant frequencies result in lower losses and are less influenced by clutter. A lower damping factor results in a better quality factor (see Equation 4.3), which means better frequency selectivity of the tag.

The standard Printed Circuit Board substrate is FR-4. This material has a relatively high dielectric permittivity ($\epsilon_r = 4.4$), but is overall not recommended to use in the high gigahertz range , due its higher losses above 1 GHz [52]. Instead, other dielectric materials are used. One of these is a ceramic laminate known as Rogers RO4003. This material's dielectric losses stay stable till far above the one gigahertz, making it much more suitable for high frequency applications [53]. For several substrates the performance of a triangular microstrip antenna was measured by Khan et al. [54]. This research showed that at 10 Gigahertz, the radiation efficiency could be increased by 20% by using RO4003 or a similar substrate instead of conventional FR-4.

A very big weakness of using other substrates is the price increase. A standard PCB can be ordered for a mere three euro's. If not bought in bulk, printing on RO4003 costs approximately 140 euros. This can be brought down to 10 euros per PCB plate when hundred are bought. Since 20 percent better performance does not make up for a 70 higher price in case of proof of concept, the tag was printed on FR-4. It was assumed that the performance benefits did not outweigh the extra costs associated with this material, given that only a proof of concept needs to be provided.

### 6.1.2. Tag size

In the self-constructed algorithm described in subsection 4.5.4, the size of the tag will be scaled down from the 3.4 by 6.4 millimeter used in the paper. A very important consideration with scaling is that most PCB fabrication companies can ensure a minimum resolution of 0.09 millimeters. In the paper, the gap between the fragments and open loop (see $d$ in Figure 4.8), is 0.1 millimeter. If the entire tag is scaled, this gap will become even smaller, which is undesirable. To solve this issue, there is four things that could be considered.

- The amount of fragments in the tag can be scaled down. This, of course, has influence on the number of possible designs. This could be an undesirable side effect of this method, leaving less possibilities for optimization.
- The tag can be scaled linearly, but the critical dimensions, such as the gap can be hard-coded to be at least 0.1 millimeter. This method works until the fragments themselves reach a length or width below 0.1 millimeter. Because in this case, the absence of one fragment in between two present fragments also results in a tolerance below 0.1 millimeter.
- The third option is a variation on the second option, but then the created matrix is not shifted by 0.1 millimeter. This already solves the risks of being below the threshold on one side of the tag. However, it still creates the same problem as the second option when fragment sizes are too small.
- A fourth option would be to move to a different production process. In the next subsection, a possible alternative using lithography is given.

### 6.1.3. Alternative production process

When the tolerances of the tag reach the limit of what is possible on a printed circuit board, other production processes have to be found. This is the case for the fragmented loop resonator as well. As is discussed in the previous subsection, the impact of scaling on the tolerances can be mitigated. However, if technology allows to scale down the tag to hundreds a few millimeters or even micrometers, further mitigation will influence the tag's performance.

Photolithography is a very common production process in microelectronics. In several cases, it has been used for the production of chipless RFID tags [55][56]. As this technology keeps on advancing, this process will become cheaper and cheaper [57]. Especially since the tag only needs one cycle of photolithography, whereas many other devices will need much more. The process for the production of an open loop resonator is visualized in Figure 6.1. The process starts off with a standard silicon wafer, laminated with a material that is suitable for high frequency RF applications. Subsequently, a layer of photoresist is spin coated over the waver. The photoresist is then developed. Since the chips will not reach a submicron scale, cheaper lithography processes can be used. After the development of the photoresist, a layer of copper will be sputtered over the wafer, as can be seen in (d) of Figure 6.1. The next step is the Chemical Mechanical Polishing of the copper and photoresist, which leaves a thin layer of copper on top of the wafer. As a final step, the remaining photoresist will be washed away using acetone.

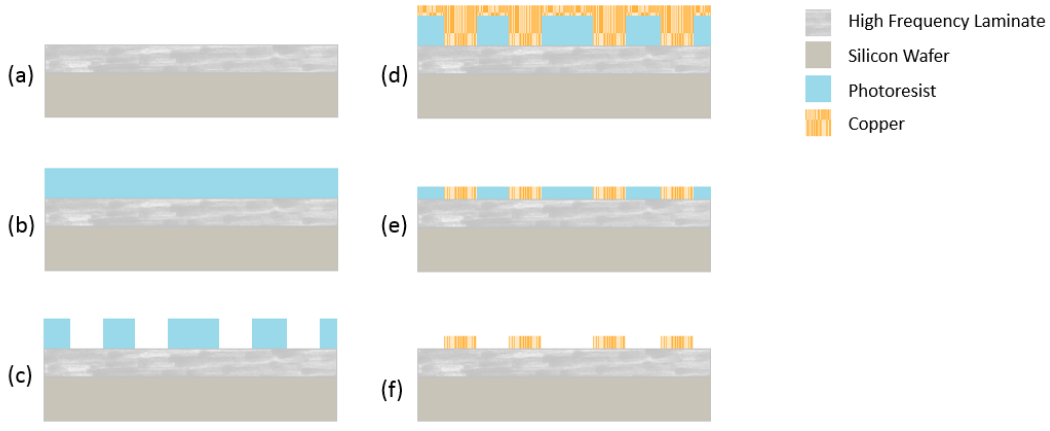


Figure 6.1: An alternative production process using photolithography

## 6.2. Realization

After taking all the design choices in consideration, the tags were produced on a standard 4-layer FR-4 substrate with copper tracing by JLCPCB [58]. The details of the design can be seen in Appendix E. After receiving the tags, they were scrubbed with sandpaper to equalize the copper structure. The result of this can be seen in Figure 6.2. Later, it was found that by insulating the tags without tin, higher resolutions can be reached (see Figure 6.2(c). The entire PCB can be seen in Figure 6.3(a). Holes were placed in the middle of the PCB to simplify breaking the PCB into individual tags. Furthermore, each tag has got its expected resonance frequency printed on the back, as is indicated in Figure 6.3(b).

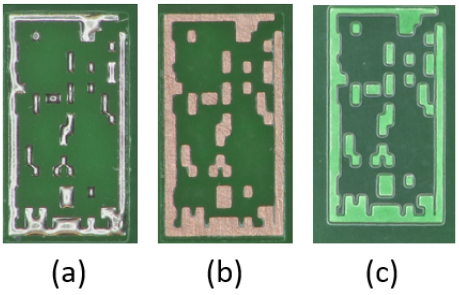


Figure 6.2: One of the RFID tags (a) tinned , (b) sanded and (c) insulated.

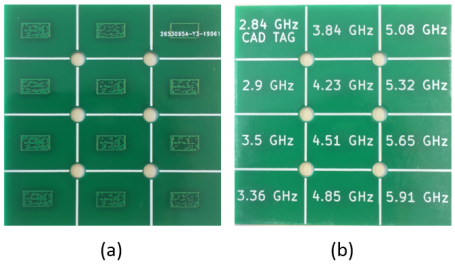


Figure 6.3: The front (a) and back (b) of the printed circuit board before broken down into individual tags

## 6.3. Testing

After receiving the tags, each was tested thoroughly. This was not only in order to characterize the tag itself, but also to verify the entire system. First, the Radar Cross Section of the tag was characterized with a network analyzer. Subsequently, the tag's response was measured using a setup with horn antennas. Finally, the system was tested using the vivaldi antennas designed inm [10]. In this section, the RCS measurements will be discussed. The other measurements affect the entire system and are discussed in [11].

### 6.3.1. RCS Measurements

Measuring the Radar Cross Section of the open loop resonator is a complex task. It namely requires a rigorous calibration phase before the Radio Cross Section is measured. The calibration techniques used for these tests are based on [24, 59], using a sphere and metal plate as references. The entire measurement report can be found in Appendix B

All the measurements showed mostly noise, and no coherent signal at their simulated RCS peaks. It could have been that the tag was too far from the antennas, and that its signal reach is below one meter. Especially since the tests were done in a room that was not entirely noise free, it is plausible that the signal drowned in the noise and was unretrievable. This is likely what happened as the reference measurements with a conductive sphere or plate only showed a maximum 15 dB increase in the S12 parameter while the difference with tag's RCS is much smaller. Unfortunately, it was not possible to perform any new measurements within the time of this thesis.

# 7

# Discussion

As can be read in [11], the response of the system cannot yet be measured. It seems that the tag is either irresponsive or the signal is drowning in noise.

If the detection problem is due to the tag, several causes can be identified. First, it could be that the resolution of the realised tag is too low. When looked under the microscope, one can see that the corners of the tag are rounded off. It could be the case that these rounded corners change the structure so much, that their response is not comparable to the simulated response. This could, for example, mean that the tag's response is shifted to a frequency outside of the ultra-wideband. Another issue with the tag could be its substrate. The tag is printed on FR-4, which has increased losses in the gigahertz range. It was found that losses can be decreased by 20 percent if high frequency laminates like the Rogers 4000 series are used. This might be a significant improvement in the tag's response.

Except for the tag there are also some problems with the rest of the system, since the larger dipole tags could not be detected either. To have a better chance of detecting the tag, the signal-to-noise ratio has to be increased. This can be done by either minimising reflections or by transmitting a stronger signal. The pulse generator of the time domain sampler and the network analyser both do not output a lot of power. By placing an amplifier in the output path of these instruments, more energy will be pushed into the tags, possibly extending its response time. This could be the difference between seeing a tag and seeing noise. But, increasing the output power will also increase reflections.

The antenna polarisation isolation has been tested to be quite poor, especially at the higher frequencies. It it not sure whether this is due to the measurement setup or the actual values. To exclude one of these, a measurement should be done in an anechoic chamber.Besides this polarisation isolation measurement, it would be more precise if all measurement are done in an anechoic chamber, even though they may seem correct at first. This includes both the antenna measurements and the tag measurements, to minimise clutter. Unfortunately, this anechoic chamber was not available during the Bachelor's Thesis time window at the TU Delft.

# 8

# Conclusion and Future Recommendations

In this thesis, a passive and chipless RFID system for sediment research is proposed. The system is intended to be deployed in Bolivia, where a semi-arid river with one source and one sink allows for the creation of a quantitative model where sediment particle size is related to bedload transport. This model requires individually distinguishable tags that reach the size of sand grains.

The designed tags use a Multiobjective Evolutionary Algorithm based on Decomposition combined with Enhanced Genetic Operators to miniaturise open-loop resonators with a fragmented base. Using this method, the tag reached a size of four by four millimeters. The designed tags operate in the ultra-Wide Band and have resonant frequencies between three and seven gigahertz. The quality factor of the optimised tags could reach approximately 130.

Antennas that are suited for use with ultra-wideband and provide a uniform phase center have been designed. The antennas have been tested to function correctly. Parameters such as the directivity and $S11$ parameter have been simulated and tested, and provide satisfying results. Some uncertainties remain about the polarisation isolation, but this requirement was stated to be of medium priority. Overall, the antennas are deemed to be suited for use in the electronic markers project.

During the final system testing, it was not yet possible to find the tags in the response produced by the test setup. It is not yet clear as why this is the case. No conclusions can be drawn yet because of this uncertainty: individual components are shown to work in simulations, and the antennas have been measured. Larger resonating tags have been tested and commercial antennas have been used. This still gave no decisive conclusion.

All in all, the project should not be considered a failure. Major progress has been made in the research of using RFID in sediment research. Although this implementation might not work, the alternative designs that are proposed in this thesis can be further explored.

# Glossary

**BAP** Bachelor Graduation Project

**EM** electromagnetic

**GPS** global positioning system

**IC** integrated circuit

**mmW** millimeter-wave

**plane wave approximation** An approximation of (electromagnetic) waves which is valid when a wave source is far away and does not encounter small objects in comparison to the wavelength

**RCS** radar cross-Section

**REE** rare earth elements

**RFID** Radio-Frequency Identification

**TDR** time-domain reflectometry

**UWB** Ultra-wideband: term to describe radio communications systems that utilises a large bandwidth, usually more than 50% of the center frequency

# Bibliography


[1] Ramon Batalla, Alison Collins, Heinz Glindemann, Sjoerd Hoornstra, Harald Köthe, Phil Owens, and John Quinton. The importance of sediment and sediment processes for river basin management. *European Sediment Research Network*, 2018. URL https://sednet.org/download/WG4_riverbasin.pdf.

[2] Chun Kiat Chang, Aminuddin Ab Ghani, Rozi Abdullah, and Nor Zakaria. Sediment transport modeling for kulim river – a case study. *Journal of Hydro-environment Research*, 2:47–59, 09 2008. doi: 10.1016/j.jher.2008.04.002.

[3] Kevin S. Black, Sam Athey, Peter Wilson, and Darren Evans. The use of particle tracking in sediment transport studies: a review. *Geological Society, London, Special Publications*, 274(1):73–91, 2007. ISSN 0305-8719. doi: 10.1144/GSL.SP.2007.274.01.09. URL https://sp.lyellcollection.org/content/274/1/73.

[4] Gema Guzmán, John Quinton, Mark Nearing, Lionel Mabit, and J Gómez. Sediment tracers in water erosion studies: Current approaches and challenges. *Journal of Soils and Sediments*, 13, 04 2013. doi: 10.1007/s11368-013-0659-5.

[5] Margot Chapuis, Christina J. Bright, John Hufnagel, and B.J. Macvicar. Detection ranges and uncertainty of passive radio frequency identification (rfid) transponders for sediment tracking in gravel rivers and coastal environments. *Earth Surface Processes and Landforms*, 39, 12 2014. doi: 10.1002/esp.3620.

[6] Bright, Christina Jane. Development of an rfid approach to monitoring bedload sediment transport and a field case study, 2014. URL http://hdl.handle.net/10012/8375.

[7] Klaus Finkenzeller. *RFID Handbook: Fundamentals and Applications in Contactless Smart Cards and Identification*. Wiley, third edition edition, 2010.

[8] Axel Decourtye, James Devillers, Pierrick Aupinel, François Brun, Camille Bagnis, Julie Fourrier, and Monique Gauthier. Honeybee tracking with microchips: a new methodology to measure the effects of pesticides. *Ecotoxicology*, 20(2):429–437, Mar 2011. ISSN 1573-3017. doi: 10.1007/s10646-011-0594-4. URL https://doi.org/10.1007/s10646-011-0594-4.

[9] Jiaguang Li, Stefan M. Luthi, Marinus Eric Donselaar, Gert Weltje, Maarten Prins, and Menno Bloemsma. An ephemeral meandering river system: Sediment dispersal processes in the río colorado, southern altiplano plateau, bolivia. *Zeitschrift für Geomorphologie*, 59, 12 2014. doi: 10.1127/zfg/2014/0155.

[10] A.S. Roos and M.A Postma. Electronic markers for geological research: Transceiverhardwaredesign. Technical report, Delft university of technology, 2019.

[11] D. de Groot and E. van der Meijs. Electronic markers for geological research: Signal processing. Technical report, Delft university of technology, 2019.

[12] A. Terry Bahill, B Bentz, and F F. Dean. Discovering system requirements. 01 2009.

[13] Jerry J Lou, Gary Andrechak, Michael Riben, and William H Yong. A review of radio frequency identification technology for the anatomic pathology or biorepository laboratory: Much promise, some progress, and more work needed. *Journal of pathology informatics*, 2:34, 08 2011. doi: 10.4103/2153-3539.83738.

[14] Y. A. Alshoudokhi, S. A. Alshebeili, M. A. Ashraf, M. R. AlShareef, and H. M. Behairy. Recent developments in chipless ultra-wide-band (uwb) radio frequency identification (rfid) systems. In *2017 IEEE 2nd Advanced Information Technology, Electronic and Automation Control Conference (IAEAC)*, pages 535–538, March 2017. doi: 10.1109/IAEAC.2017.8054072.

[15] N. C. Karmaker. Tag, you're it: Radar cross section of chipless rfid tags. *IEEE Microwave Magazine*, 17(7):64–74, July 2016. ISSN 1527-3342. doi: 10.1109/MMM.2016.2549160.

[16] C. Matzler. Microwave permittivity of dry sand. *IEEE Transactions on Geoscience and Remote Sensing*, 36(1):317–319, Jan 1998. ISSN 0196-2892. doi: 10.1109/36.655342.

[17] P. R. Lacko, W. W. Clark, K. Sherbondy, J. M. Ralston, and E. Dieguez. Studies of ground penetrating radar antennas. In *Proceedings of the 2nd International Workshop onAdvanced Ground Penetrating Radar, 2003.*, pages 24–29, May 2003. doi: 10.1109/AGPR.2003.1207287.

[18] Q. Wang, Z. An, Y. Yang, and C. Su. Emi principle and suppression method in vehicle ignition system. In *2012 Sixth International Conference on Electromagnetic Field Problems and Applications*, pages 1–4, June 2012. doi: 10.1109/ICEF.2012.6310311.

[19] Christian Ho, Stephen Slobin, Anil Kantak, and Sami Asmar. Solar brightness temperature and corresponding antenna noise temperature at microwave frequencies. *Interplanetary Network Progress Report*, 11 2008.

[20] H. Dagan, A. Shapira, A. Teman, A. Mordakhay, S. Jameson, E. Pikhay, V. Dayan, Y. Roizin, E. Socher, and A. Fish. A low-power low-cost 24 ghz rfid tag with a c-flash based embedded memory. *IEEE Journal of Solid-State Circuits*, 49(9):1942–1957, Sep. 2014. ISSN 0018-9200. doi: 10.1109/JSSC.2014.2323352.

[21] A. Y. Jou, H. Shan, H. Pajouhi, J. Peterson, and S. Mohammadi. A single-chip wireless powered rfid antenna and transceiver. *IEEE Journal of Radio Frequency Identification*, 1(3):219–227, Sep. 2017. ISSN 2469-7281. doi: 10.1109/JRFID.2017.2789246.

[22] D. Micheli, A. Vricella, R. Pastore, and M. Marchetti. Synthesis and electromagnetic characterization of frequency selective radar absorbing materials using carbon nanopowders. *Carbon*, 77:2326–2337, June 2014.

[23] I. Jalaly and I. D. Robertson. Capacitively-tuned split microstrip resonators for rfid barcodes. In *2005 European Microwave Conference*, volume 2, pages 4 pp.–1164, Oct 2005. doi: 10.1109/EUMC.2005.1610138.

[24] Romain Siragusa Pierre Lemaître-Auger Olivier Rance, Etienne Perret. *RCS Synthesis for Chipless RFID: Theory and Design*. Elsevier, first edition edition, 2017.

[25] Lu Zhang, S. Rodriguez, H. Tenhunen, and Li-Rong Zheng. An innovative fully printable rfid technology based on high speed time-domain reflections. In *Conference on High Density Microsystem Design and Packaging and Component Failure Analysis, 2006. HDP'06.*, pages 166–170, June 2006. doi: 10.1109/HDP.2006.1707587.

[26] Kimmo Rasilainen and Ville V. Viikari. Transponder designs for harmonic radar applications. *International Journal of Antennas and Propagation*, 2015, May 2015.

[27] G. Marrocco. The art of uhf rfid antenna design: impedance-matching and size-reduction techniques. *IEEE Antennas and Propagation Magazine*, 50(1):66–79, Feb 2008. ISSN 1045-9243. doi: 10.1109/MAP.2008.4494504.

[28] H. Wheeler. Small antennas. *IEEE Transactions on Antennas and Propagation*, 23(4):462–469, July 1975. ISSN 0018-926X. doi: 10.1109/TAP.1975.1141115.

[29] T. K. Lo, Chun-On Ho, Y. Hwang, E. K. W. Lam, and B. Lee. Miniature aperture-coupled microstrip antenna of very high permittivity. *Electronics Letters*, 33(1):9–10, Jan 1997. ISSN 0013-5194. doi: 10.1049/el:19970053.

[30] Hanna Kähäri, Prasadh Ramachandran, Jari Juuti, and Heli Jantunen. Room-temperature-densified li2moo4 ceramic patch antenna and the effect of humidity. *International Journal of Applied Ceramic Technology*, 14(1):50–55, 2017. doi: 10.1111/ijac.12615. URL `https://ceramics.onlinelibrary.wiley.com/doi/abs/10.1111/ijac.12615`.

[31] L. Wang, T. Liu, J. Sidén, and G. Wang. Design of chipless rfid tag by using miniaturized open-loop resonators. *IEEE Transactions on Antennas and Propagation*, 66(2):618–626, Feb 2018. ISSN 0018-926X. doi: 10.1109/TAP.2017.2782262.

[32] A. Vena, E. Perret, B. Sorli, and S. Tedjini. Theoretical study on detection distance for chipless rfid systems according to transmit power regulation standards. In *2015 9th European Conference on Antennas and Propagation (EuCAP)*, pages 1–4, April 2015.

[33] D.A.E. de Gruijl and M. Kraaijeveld. Electronic markers for geological research: Tag design. Technical report, Delft university of technology, 2019.

[34] Reza Rezaiesarlak and Majid Manteghi. *CHIPLESS RFID*. Springer, 2016.

[35] Chester K. Wentworth. A scale of grade and class terms for clastic sediments. *The Journal of Geology*, 30 (5):377–392, 1922. ISSN 00221376, 15375269. URL `http://www.jstor.org/stable/30063207`.

[36] Michael T. Tulley Eugene F. Knott, John F. Schaeffer. *Radar Cross Section*. SciTech Publishing, 2004.

[37] Roselena Faez Marcelo Miacci Evandro Nohara Mirabel Rezende, Inácio Martin. Radar cross section measurements (8-12 ghz) of magnetic and dielectric microwave absorbing thin sheets. *Revista de Fisica Aplicada e Instrumentacão*, 15(1):24–29, Decembe 2002.

[38] R. Rezaiesarlak and M. Manteghi. Complex-natural-resonance-based design of chipless rfid tag for high-density data. *IEEE Transactions on Antennas and Propagation*, 62(2):898–904, Feb 2014. ISSN 0018-926X. doi: 10.1109/TAP.2013.2290998.

[39] Da-Wei Ding and Gang Wang. Moea/d-go for fragmented antenna design. *Progress In Electromagnetics Research*, 33:1–15, 2013. doi: 10.2528/PIERM13071610.

[40] Stevan Preradovic, Isaac Balbin, Nemai Karmakar, and Gerhard (Gerry Swiegers. Multiresonator-based chipless rfid system for low-cost item tracking. *Microwave Theory and Techniques, IEEE Transactions on*, 57:1411 – 1419, 06 2009. doi: 10.1109/TMTT.2009.2017323.

[41] Ali Jalal. Passive rfid tags. *Wulfenia*, 22:415–435, 12 2015.

[42] Jia-Sheng Hong and M. J. Lancaster. Couplings of microstrip square open-loop resonators for cross-coupled planar microwave filters. *IEEE Transactions on Microwave Theory and Techniques*, 44(11):2099–2109, Nov 1996. ISSN 0018-9480. doi: 10.1109/22.543968.

[43] R. Dinesh, P. V. Anila, C. M. Nijas, M. Sumi, and P. Mohanan. Open loop multi-resonator based chipless rfid tag. In *2014 XXXIth URSI General Assembly and Scientific Symposium (URSI GASS)*, pages 1–4, Aug 2014. doi: 10.1109/URSIGASS.2014.6929436.

[44] Ayman S. Al-zayed and Shameena V.A. Novel chipless rfid technology using open loop resonator. *Atlantis Press*, pages 81–83, 2016.

[45] V. Sharma and M. Hashmi. Chipless rfid tag based on open-loop resonator. In *2017 IEEE Asia Pacific Microwave Conference (APMC)*, pages 543–546, Nov 2017. doi: 10.1109/APMC.2017.8251502.

[46] Dawei Ding, Xiao-Dong Ding, Jing Xia, and Lixia Yang. Moea/d-go+fdtd for optimization design of fragment-type structure. 2017.

[47] Qi Zhao, Gang Wang, and Dawei Ding. Compact microstrip bandpass filter with fragment-loaded resonators. *Microwave and Optical Technology Letters*, 56(12):2896–2899, 2014. doi: 10.1002/mop.28726. URL `https://onlinelibrary.wiley.com/doi/abs/10.1002/mop.28726`.

[48] Q. Zhang and H. Li. Moea/d: A multiobjective evolutionary algorithm based on decomposition. *IEEE Transactions on Evolutionary Computation*, 11(6):712–731, Dec 2007. ISSN 1089-778X. doi: 10.1109/TEVC.2007.892759.

[49] S. Mostapha Kalami Heris. Moea/d in matlab. `https://yarpiz.com/95/ypea124-moead`, 2014.

[50] Charles Darwin. *On the Origin of Species by Means of Natural Selection*. Murray, London, 1859. or the Preservation of Favored Races in the Struggle for Life.

[51] Ansoft. Hfss. URL `https://www.ansys.com/products/electronics/ansys-hfss`.

[52] *NEMA Standards Publication No. LI 1-1998*. National Electrical Manufacturers Association.

[53] *RO40000 Series: High Frequency Circuit Materials*. Rogers datasheet.

[54] Anzar Khan and Rajesh Nema. Analysis of five different dielectric substrates on microstrip patch antenna. *International Journal of Computer Applications*, 55:40–47, 10 2012. doi: 10.5120/8826-2905.

[55] Raji Nair, Marvin Barahona, Diego Betancourt, Georg Schmidt, Maxi Bellmann, Daniel Höft, Dirk Plettermeier, Arved C. Huebler, and Frank Ellinger. A novel fully printed 28-bits capacity chipless rfid tag based on open conical resonators. pages 2219 – 2222, 08 2014.

[56] Nemai Karmakar, Mohammad Zomorrodi, and C Divarathne. *Advanced Chipless RFID: Imaging 60 GHz MIMO / ML Detection*. 08 2016. doi: 10.1002/9781119227342.

[57] Ravi Panwar. Recent developments, issues and challenges for lithography in ulsi fabrication, journal = Atlantis Press. 1(2):702–711, 2016.

[58] Jlcpcb impedence controlled specifications. URL `https://jlcpcb.com/client/index.html#/impedance`.

[59] W. Wiesbeck and S. Riegger. A complete error model for free space polarimetric measurements. *IEEE Transactions on Antennas and Propagation*, 39(8):1105–1111, Aug 1991. ISSN 0018-926X. doi: 10.1109/8.97343.

# A

# Scripts

Listing A.1: CAD stl structure generator

```
%Project:    Electronic Markers for Geological Research
%Subject:    CAD structure generator
%Author:     de Gruijl, D.A.E. and Kraaijeveld, M..
%Date:       18-5-2019

%MATLAB Sources for stl generators.
% https://uk.mathworks.com/matlabcentral/fileexchange/27733-converting-a-3d-logical
%-array-into-an-stl-surface-mesh
% https://uk.mathworks.com/matlabcentral/fileexchange/20922-stlwrite-write-ascii-or-binary-stl-files

 close all
 clear
 clc


%This matrix describes the loaded fragments described in the paper by
%Wang et al.
OptMat = [0   1   1   1   1   1   1   1   1   1   1   0   1   1   1   0   1   1   0   0
          1   0   0   1   0   0   0   0   0   0   0   0   0   1   0   0   0   0   0   0
          1   1   1   0   0   0   1   1   1   0   1   0   0   0   0   0   1   0   0   0
          1   0   0   1   0   1   1   0   1   1   0   1   1   0   0   1   1   0   1   1
          1   1   0   0   0   0   1   1   0   1   1   0   0   0   1   1   0   0   1   1
          0   0   0   0   0   1   0   0   0   0   1   0   1   1   0   1   0   0   0   1
          1   0   0   0   0   1   0   0   0   0   1   0   1   1   0   1   0   0   0   1
          1   0   1   1   1   1   1   0   1   1   1   1   0   1   0   1   0   0   1   0
          1   0   1   1   0   1   1   1   1   1   1   1   1   1   1   1   1   0   0   0
          1   0   0   0   0   0   0   0   0   0   1   0   1   0   0   1   0   0   0   1
          0   1   0   0   1   1   0   0   0   0   0   0   1   0   0   1   0   0   1   1
          1   0   0   1   1   1   0   0   0   0   1   0   0   1   0   1   0   1   1   1
          1   0   0   0   0   1   0   0   1   0   1   0   1   1   0   1   0   1   0   1
          1   1   0   0   1   1   1   1   1   1   0   1   1   0   1   0   1   0   0   0
          1   1   0   1   1   0   0   0   0   0   1   1   0   0   1   1   1   1   1   0];

%The orientation of the matrix 180 degrees twisted.
OptMat = rot90(OptMat);
OptMat = rot90(OptMat);

%One could insert this line if no fragments are needed.
%OptMat = rand(15,20)>1.5


%Here, one could set what the dimensions are of one block in the stl file
unit = 4; %1 = 0.1mm, 2= 0.05mm , 4= 0.025mm

%Each fragment is 0.2mm in width and 0.3mm in length. This is incorporated in the code.
width =2*unit; %0.2 mm width
length = 3*unit; %0.3mm length
x = ones(width, length);
```

```
OptMat = kron(OptMat,x);



%The gap will describe with how many millimeters the matrix is shift right
%within the fixed openloop
%OLwidth describes the width of the open loop, which is 0.2 mm in the paper
gap = 1*unit;
OLwidth = 2*unit;
OptMat = padarray(OptMat,[gap 0],0,'pre');
[arrayx, arrayy] = size(OptMat);
OptMat((arrayx+1-gap):arrayx,:) = []; %deleting the row on right
OptMat = padarray(OptMat,[OLwidth OLwidth],1,'both');

[totx, toty] = size(OptMat);

for i = 1:OLwidth
    for j = 1:(length+OLwidth)
        OptMat(i,j)=0;
    end
end

%HFSS will crash if two structures are only connected by one corner.
%This function will "repair" the structure in such a way that all fragments are connected.
for j = 1:(toty-1)
    for i = 1:(totx-1)
        if (OptMat(i,j)==1 && OptMat(i,j) == OptMat((i+1),(j+1)) && OptMat(i+1,j)==0 && OptMat(i,j+1)==0)
            OptMat(i,j+1) = 1;
            OptMat(i+1,j) = 1;
        end
    end
end

for j = 1:(toty-1)
    for i = 2:totx
     if (OptMat(i,j)==1 && OptMat(i,j) == OptMat((i-1),(j+1)) && OptMat(i-1,j) == 0 && OptMat(i,j+1) == 0)
            OptMat(i,j+1) = 1;
            OptMat(i-1,j) = 1;
     end
    end
end




%with "thickness" we create a 3D matrix of zeros and ones.
thickness = 2;
OptMat3D = repmat(OptMat, [1,1,thickness]);
[x, y, z] = size(OptMat3D);

%Here, the widht, length and thickness of the resonator is determined.
gridx = linspace(0,(3.4),x);
gridy = linspace(0,(6.4),y);
gridz = linspace(0,0.035,z);

%The script to convert a 3D binary matrix into an stl file.
[faces, vertices] = CONVERT_voxels_to_stl('OpenLoopResonator.stl',OptMat3D, gridx, gridy, gridz,'ascii');


%Plotting the Figure
SmartFigure = ~OptMat3D;
figure;
imagesc(squeeze(sum(SmartFigure,3)));
colormap(gray);
axis off

%Plotting the stl file
figure
[stlcoords] = READ_stl('OpenLoopResonator.stl');
xco = squeeze( stlcoords(:,1,:) )';
yco = squeeze( stlcoords(:,2,:) )';
```

```
zco = squeeze( stlcoords(:,3,:) )';
[hpat] = patch(xco,yco,zco,'b');
axis equal


%% The option to reduce the size of the stl file
% [xpat] = reducepatch (hpat, 0.001);
%
% stlwrite('reduced.stl',xpat);
% figure
% [stlcoords2] = READ_stl('reduced.stl');
% xco2 = squeeze( stlcoords2(:,1,:) )';
% yco2 = squeeze( stlcoords2(:,2,:) )';
% zco2 = squeeze( stlcoords2(:,3,:) )';
% [hpat2] = patch(xco,yco,zco,'b');
% axis equal
```

Listing A.2: MOEA/D-GO main script

```
% Adapted to MOEA/D-go by M. Kraaijeveld
% Copyright (c) 2015, Yarpiz (www.yarpiz.com)
% All rights reserved. Please read the "license.txt" for license terms.
%
% Project Code: YPEA124
% Project Title: Implementation of MOEA/D
% Muti-Objective Evolutionary Algorithm based on Decomposition
% Publisher: Yarpiz (www.yarpiz.com)
%
% Developer: S. Mostapha Kalami Heris (Member of Yarpiz Team)
%
% Contact Info: sm.kalami@gmail.com, info@yarpiz.com
%

clc;
clear;
close all;

%% Problem Definition

CostFunction=@(x) ZDT(x);  % Cost Function

numx = 15;
numy = 15;                % Number of Decision Variables

VarSize=[numx numy];   % Decision Variables Matrix Size

VarMin = 0;          % Decision Variables Lower Bound
VarMax = 1;          % Decision Variables Upper Bound

nObj=4;

%% MOEA/D Settings

MaxIt=100;  % Maximum Number of Iterations

nPop=30;    % Population Size (Number of Sub-Problems)

nArchive=30;

T=max(ceil(0.15*nPop),2);     % Number of Neighbors
T=min(max(T,2),15);

crossover_params.gamma=0.5;
crossover_params.VarMin=VarMin;
crossover_params.VarMax=VarMax;
mutprob=0.01;

%% Initialization

% Create Sub-problems
```

```
sp=CreateSubProblems(nObj,nPop,T);

% Empty Individual
empty_individual.Position=[];
empty_individual.Cost=[];
empty_individual.g=[];
empty_individual.IsDominated=[];

% Initialize Goal Point
%z=inf(nObj,1);
z=zeros(nObj,1);

% Create Initial Population
pop=repmat(empty_individual,nPop,1);
for i=1:nPop
    pop(i).Position=unifrnd(VarMin,VarMax,VarSize)>0.5;
    pop(i).Cost=CostFunction(pop(i).Position);
    z=min(z,pop(i).Cost);
end

for i=1:nPop
    pop(i).g=DecomposedCost(pop(i),z,sp(i).lambda);
end

% Determine Population Domination Status
pop=DetermineDomination(pop);

% Initialize Estimated Pareto Front
EP=pop(~[pop.IsDominated]);

%% Main Loop

for it=1:MaxIt
    for i=1:nPop

        % Reproduction (Crossover)
            K=randsample(T,1);

        j1=sp(i).Neighbors(K);
        % select random neighbor
        p1=pop(j1);
        % select best neighbor
        [M,j2]=min([pop(sp(i).Neighbors).g]);
        p2=pop(sp(i).Neighbors(j2));
        % current individual
        p3=pop(i);

        y=empty_individual;
        y.Position=Crossover(p1.Position,p2.Position,p3.Position,numx,numy);
        % mutation
        y.Position=Mutation(numx,y.Position,mutprob);
        %determine offspring cost
        y.Cost=CostFunction(y.Position);

        z=min(z,y.Cost);
        %check if offspring outperforms population
        for j=sp(i).Neighbors
            y.g=DecomposedCost(y,z,sp(j).lambda);
            if y.g<=pop(j).g
                pop(j)=y;
            end
        end

    end

    % Determine Population Domination Status
        pop=DetermineDomination(pop);

    ndpop=pop(~[pop.IsDominated]);

    EP=[EP
```

```
        ndpop]; %#ok

    EP=DetermineDomination(EP);
    EP=EP(~[EP.IsDominated]);

    if numel(EP)>nArchive
        Extra=numel(EP)-nArchive;
        ToBeDeleted=randsample(numel(EP),Extra);
        EP(ToBeDeleted)=[];
    end

    % Plot EP
    figure(1);
    PlotCosts(EP);
    pause(0.01);


    % Display Iteration Information
    disp(['Iteration ' num2str(it) ': Number of Pareto Solutions = ' num2str(numel(EP))]);

end

%% Reults

disp(' ');

EPC=[EP.Cost];
for j=1:nObj

    disp(['Objective #' num2str(j) ':']);
    disp(['      Min = ' num2str(min(EPC(j,:)))]);
    disp(['      Max = ' num2str(max(EPC(j,:)))]);
    disp(['    Range = ' num2str(max(EPC(j,:))-min(EPC(j,:)))]);
    disp(['     St.D. = ' num2str(std(EPC(j,:)))]);
    disp(['     Mean = ' num2str(mean(EPC(j,:)))]);
    disp(' ');

end
```

Listing A.3: Cost decomposition

```
% Weighted sum decomposition for MOEA/D based on doi:10.1109/TEVC.2007.892759
% M. Kraaijeveld May 2019


function g=DecomposedCost(individual,z,lambda)

    if isfield(individual,'Cost')
        fx=individual.Cost;
    else
        fx=individual;
    end

    g=sum(lambda.*fx);

end
```

[frame=single,language=Matlab,caption=Cost determination]chapters/04:Appendix/ZDT.m

Listing A.4: HFSS simulation script

```
' ----------------------------------------------
' Script Recorded by Ansoft HFSS Version 13.0.2
' 3:41:27 PM  Jun 04, 2019
' ----------------------------------------------
Dim oAnsoftApp
Dim oDesktop
Dim oProject
Dim oDesign
Dim oEditor
Dim oModule
```

```
Set oAnsoftApp = CreateObject("AnsoftHfss.HfssScriptInterface")
Set oDesktop = oAnsoftApp.GetAppDesktop()
oDesktop.RestoreWindow
oDesktop.OpenProject "O:\michaelkraaije\...\Optimisation.hfss"
Set oProject = oDesktop.SetActiveProject("Optimisation")
Set oDesign = oProject.SetActiveDesign("HFSSDesign2")
Set oEditor = oDesign.SetActiveEditor("3D␣Modeler")
oEditor.Delete Array("NAME:Selections", "Selections:=", "MooiDingetje")
oEditor.Import Array("NAME:NativeBodyParameters", "HealOption:=", 0, "CheckModel:=", _
false, "Options:=", "0", "FileType:=", "UnRecognized", "MaxStitchTol:=", -1, "ImportFreeSurfaces:=", _
false, "SourceFile:=", "O:\michaelkraaije\...\MooiDingetje.stl")
oEditor.AssignMaterial Array("NAME:Selections", "Selections:=", "MooiDingetje"), Array("NAME:Attributes",
"MaterialValue:=", _
"" & Chr(34) & "copper" & Chr(34) & "", "SolveInside:=", false)
oEditor.HealObject Array("NAME:Selections", "Selections:=", "MooiDingetje", "NewPartsModelFlag:=", _
"Model"), Array("NAME:ObjectHealingParameters", "Version:=", 1, "AutoHeal:=", true, "TolerantStitch:=", _
true, "SimplifyGeom:=", true, "TightenGaps:=", true, "StopAfterFirstStitchError:=", _
false, "MaxStitchTol:=", 0.001, "ExplodeAndStitch:=", true, "GeomSimplificationTol:=", _
-1, "MaximumGeneratedRadiusForSimplification:=", -1, "SimplifyType:=", 2, "TightenGapsWidth:=", _
1E-06, "RemoveSliverFaces:=", false, "RemoveSmallEdges:=", false, "RemoveSmallFaces:=", _
false, "SliverFaceTol:=", 0, "SmallEdgeTol:=", 0, "SmallFaceAreaTol:=", 0, "BoundingBoxScaleFactor:=", _
1250, "RemoveHoles:=", false, "RemoveChamfers:=", false, "RemoveBlends:=", _
false, "HoleRadiusTol:=", 0, "ChamferWidthTol:=", 0, "BlendRadiusTol:=", 0, "AllowableSurfaceAreaChange:=",
_
5, "AllowableVolumeChange:=", 5)
oProject.Save
oDesign.Analyze "Setup1␣:␣Sweep"
Set oModule = oDesign.GetModule("ReportSetup")
oModule.ExportToFile "XY␣Plot␣1", "O:\michaelkraaije\...\RCSTotal.csv"
oModule.ExportToFile "XY␣Plot␣2", "O:\michaelkraaije\...\RCSY.csv"
```

Listing A.5: Crossover operator

```
%MOEA/D-GO Crossover operation
%as decribed by Ding in Progress in
%Electromagnetics Research M . 2013, Vol. 33, p1-15
%M. Kraaijeveld May 2019

function y=Crossover(x1,x2,x3,numx,numy)

    col=randi(numy);
    y=zeros(numx,numy);
    y(:,1:col-1)=x1(:,1:col-1);
    y(:,col)=x2(:,col);
    y(:,col+1:numy)=x3(:,col+1:numy);
end
```

Listing A.6: Mutation operator

```
%Mutation operator for MEOAD-GO
%as decribed by Ding in Progress in
%Electromagnetics Research M . 2013, Vol. 33, p1-15
%M. Kraaijeveld for BAP Geological Markers 28-5-19

function y=Mutation(numx,y,prob)
    row=randi(numx);
     if rand()>1-prob
         y(row,:)=rand(1,numx)>0.5;
    end
end
```

# B

# Radar Cross Section Measurements

## B.1. Introduction

Measuring the Radaer Cross Section of the open loop resonator is a complex task. It namely requires a rigorous calibration phase before the Radar Cross Section is measured. The calibration techniques used for these tests are based on [24, 59]. The technique is based on the measurement of an empty measurement $S_{21}^{empty}$, a measurement of the tag $S_{21}^{tag}$ and a measurement of a reference object $S_{21}^{ref}$ with a known radio cross section $\sigma_{RCS}^{ref}$. The RCS is then calculated using Equation B.1

$$\sigma = \left| \frac{S_{21}^{tag} - S_{21}^{empty}}{S_{21}^{ref} - S_{21}^{empty}} \right|^2 \cdot \sigma_{RCS}^{ref} \quad (\mathrm{m}^2) \quad \text{(B.1)}$$

## B.2. Measurement Setup

The tags were measured from a meter distance, with the measurement setup visible in Figure B.2 and Figure B.1. Measuring in an anechoic chamber would have been ideal, but by using as much microwave absorbing material as possible, the noise floor is brought down.

A Hewlett-Packard 8753D vector network analyzer was connected two horn antennas with a coaxial cable using SMA connectors. This vector network analyzer was connected to a laptop with a GPIB-connector. The transmitting and receiving antenna were both placed under a small angle, with the tag exactly in its line of sight.

First, a sphere and a square metal plate were measured as known references. Then, an empty measurement was done. Finally, each tag was measured.

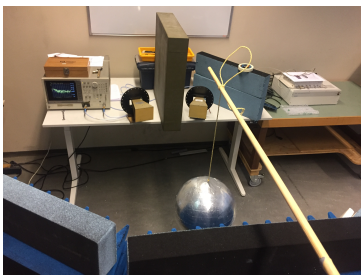

Figure B.1: The measurement setup for measuring the sphere as reference.

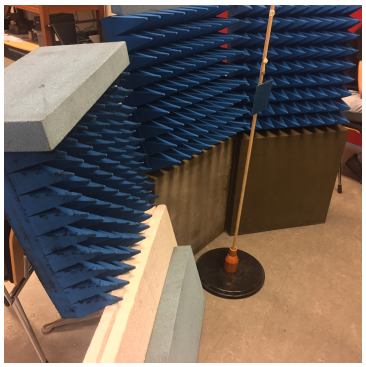

Figure B.2: The measurement setup for measuring the metal square as reference.

## B.3. Results

The results were gathered through matlab, and plotted in Figure B.3 and Figure B.4. The pictures show tag measurements for normal polarization and cross-polarization. It also includes a 'mystery tag'. If the results hold merit, it can be derived which tag the mystery tag is.

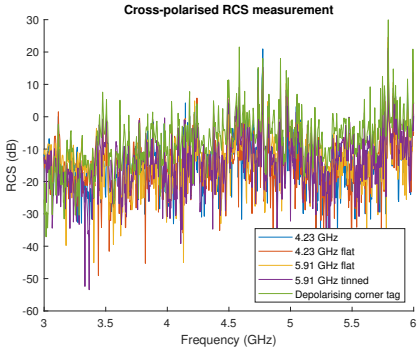


Figure B.3: Cross-polar RCS measurement

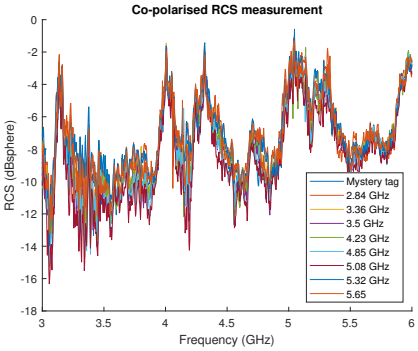


Figure B.4: Co-polar RCS measurement

## B.4. Conclusion

As we can see in the figures, the RCS plots of both normal and cross polarized signals do not show any RCS peaks at or close to the simulated resonance frequency. This means that, even though the measurement setup was thoroughly calibrated, the signal was too weak to be detected or non-existent.

The inability to measure results can have several causes.

- The tags might have stood too far from the transmitting and receiving antenna. The calculated measurement distance of the system was, but the circumstances are far from ideal. The tags might have had a much stronger signal if measured closer towards the antennas.
- The noise has not been surpressed enough. Since there was no availability of an anechoic room, it was necessary to surpress the noise in the measurement setup as much as possible. However, the lack of resources led to a far from perfect measurement setup. The noise floor could have been drawn up so high, that retrieving a signal is impossible.
- The tag itself is not radiating. This could have many reasons. First, it could be that due to inexpensive production processes, the tag has become too different from the tags that are being simulated. This difference in shape has had too much impact on its working principle, which makes the tag undetectable. Another example of technology imperfection could be the presence of FR-4 material, instead of a substrate that is better suitable for high frequencies. As is discussed in subsection 4.3.2 and section 6.1, it would be ideal if all the losses in the tag were radiating losses. However, the tag can also lose energy through its substrate. If a low-loss substrate special for high frequencies was used, the chance on significant losses due to substrate could have been lowered.

# C

# Preliminairy Tag Population

| Tag | Resonating frequency (GHz) | RCS (dBsm) |
|---|---|---|
| **1** | 4.4250 | -42.7564 |
| **2** | 7.5000 | -25.2290 |
| **3** | 7.4250 | -25.9494 |
| **5** | 6.9000 | -28.7227 |
| **6** | 7.5750 | -24.2494 |
| **7** | 6.7500 | -25.8731 |
| **8** | 6.7500 | -25.8731 |
| **9** | 6.7500 | -25.8731 |
| **10** | 7.6500 | -23.4194 |
| **11** | 7.8000 | -22.4233 |
| **12** | 6.7500 | -25.8731 |
| **13** | 7.6500 | -23.4194 |
| **14** | 7.3500 | -22.8985 |
| **15** | 7.3500 | -22.8985 |
| **16** | 7.5000 | -21.9971 |
| **17** | 7.5000 | -21.9971 |
| **18** | 7.5000 | -21.9971 |
| **19** | 7.5000 | -21.9971 |
| **20** | 7.5000 | -21.9971 |
| **21** | 7.5000 | -21.9971 |
| **22** | 7.5000 | -21.9971 |
| **23** | 7.5000 | -21.9971 |
| **24** | 7.5000 | -21.9971 |
| **25** | 7.5000 | -21.9971 |
| **26** | 7.5000 | -21.9971 |
| **27** | 7.5000 | -21.9971 |
| **28** | 7.5000 | -21.9971 |
| **29** | 7.5000 | -21.9971 |
| **30** | 7.5000 | -21.9971 |

# D

# Directionality simulations

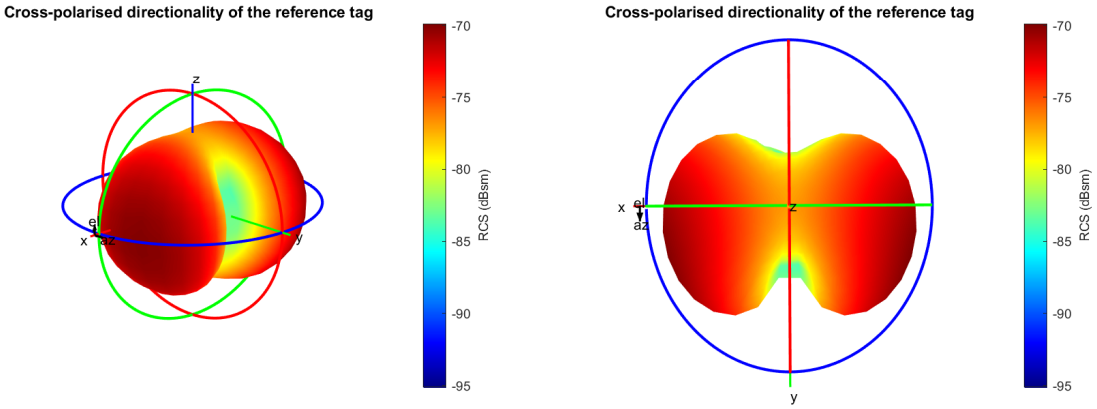


(a) (b)

Figure D.1: Cross-polarised directional properties of the reference tag at its resonance frequency

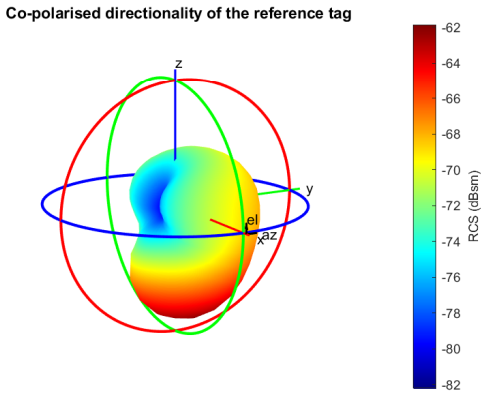


Figure D.2: Co-polarised directional properties of the reference tag at its resonance frequency

# E

# PCB Design specifications

| | Specification | Details |
|---|---|---|
| **Layer** | 4 Layer | |
| **Material** | FR-4 | |
| **Dimensions** | 45 mm × 45 mm | |
| **Solder mask** | LPI | Liquid Photo-Imageable solder mask |
| **Board thickness** | 1.6 mm | |
| **Copper thickness** | 0.035 mm | |
| **Minimal trace width** | 0.0889 mm | |
| **Minimal spacing width** | 0.0889 mm | |